Int J Coal Sci Technol (2021) 8(1):23–46
https://doi.org/10.1007/s40789-020-00336-x

Analysis of solid sorbents for control and removal processes for elemental mercury from gas streams: a review

Piotr Kunecki[1] · Dorota Czarna-Juszkiewicz[1] · Magdalena Wdowin[1]

Received: 17 October 2019 / Revised: 5 May 2020 / Accepted: 28 May 2020 / Published online: 22 June 2020

Abstract Due to the restriction such as the Minamata Convention as well as the IED of the European Commission, mercury removal from flue gases of coal-fired power plants (CPP) is an increasingly important environmental issue. This makes this topic very crucial for both the energy industry and scientists. This paper shows how mercury arises from natural resources, i.e., coals, through their combustion processes in CPP and considers the issue of mercury content in flue gases and solid-state coal combustion by-products. The main part of this paper presents a review of the solid sorbents available for elemental mercury control and removal processes, tested on a laboratory scale. The described solutions have a potential for wider usage in exhaust gas treatment processes in the energy production sector. These solutions represent the latest developments in the field of elemental mercury removal from gases. The authors present an overview of the wide range of solid sorbents and their modifications intended to increase affinity for Hg^0. Among the presented sorbents are the well-known activated carbon solutions but also novel modifications to these and other innovative sorbent proposals based on, e.g., zeolites, biochars, other carbon-based materials, metal-organic frameworks. The paper presents a wide range of characteristics of the described sorbents, as well as the conditions for the Hg^0 removal experiments summarizing the compendium of novel solid sorbent solutions dedicated to the removal of elemental mercury from gases.

Graphic abstract

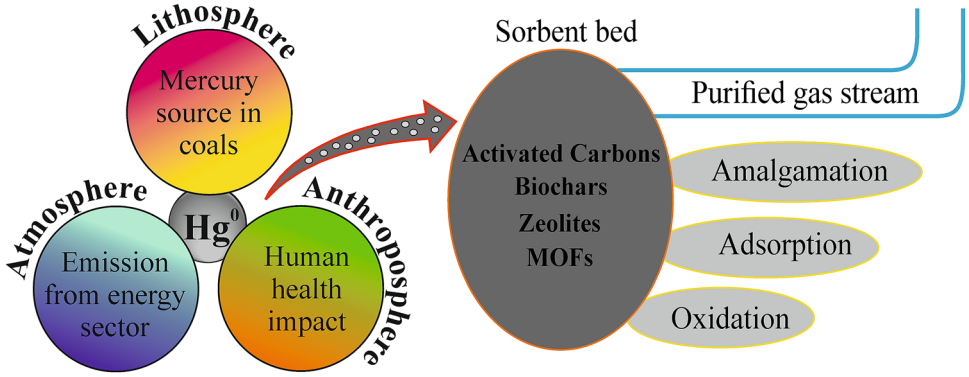

Keywords Solid sorbents · Textural properties · Elemental mercury removal · Flue gas · Gas stream

Electronic supplementary material The online version of this article (https://doi.org/10.1007/s40789-020-00336-x) contains supplementary material, which is available to authorized users.

✉ Piotr Kunecki
pkunecki@min-pan.krakow.pl

[1] Mineral and Energy Economy Research Institute, Polish Academy of Sciences, Wybickiego 7a, 31-261 Kraków, Poland

1 Introduction

Atmospheric mercury pollution from anthropogenic sources has been one of the key topics of global environmental concern in recent years. Mercury is dangerous because of its high chemical and biological activity, toxicity, persistence and volatility, as well as its long-range transportability. Once released into the environment, it remains present and is accumulated in living organisms through food chains, creating many toxic compounds, both inorganic and organic. Due to its highly bio-accumulative properties, the mercury content in the biosphere of the earth is constantly increasing. Mercury is known to be third on the list of substances most dangerous to human health drawn up by the Agency for Toxic Substances and Disease Registry (Mahaffey et al. 2012; Lavoie et al. 2013; Zhang et al. 2016) In general, in the atmosphere mercury comprises three major chemical forms. Hg^0—gaseous elemental mercury—is the most stable species, representing about 90% of total atmospheric mercury. Depending on ambient environmental conditions, its residence time is estimated to be from as little as a few hours to over a year. Usually it is several months. Oxidized Hg^{2+} is characterized as a form which is highly soluble in water. This is because this species may be relatively simply incorporated into droplets. Then, it may be adsorbed onto surfaces via wet and dry deposition. The residence time is far shorter than in the case of Hg^0. In this case it is from a few hours to several days, causing a more local environmental impact. The third mercury species is bonded to solid particles. Hg^p has an approximate residence time of hours to weeks and is characterized by a greater susceptibility to transportation over longer distances (Schroeder and Munthe 1998; Lindberg et al. 2007; Gustin et al. 2008; Fu et al. 2012). Nowadays, the main global mercury emission sources are coal combustion, cement clinker production and primary production of ferrous and non-ferrous metals (UNEP 2013a). The main fossil fuels contaminated with mercury are coal, petroleum, natural gas, shale oil and bitumen. Chemically, these are hydrocarbons, formed as a result of geological processes, from the remains of organic matter produced hundreds of millions of years ago (Chmielewski 2004). Despite the fact that world coal production decreased by 0.6% in 2014 and by a further 2.8% in 2015, coal combustion processes still provide about 40% of the world's electricity (WEC 2016). It is well recognized that coal is not a clean fuel. During the combustion processes, numerous pollutants, such as CO_2, SO_x, NO_x, VOCs (volatile organic compounds) and mercury, are released into the atmosphere (Chmielewski 2004). This branch of the energy industry also generates significant amounts of solid by-products, such as slugs, slug-ash mixtures, fly and bottom ashes and microspheres, which also contain mercury in their composition and are very harmful to the earth's ecosystems (Brown et al. 1999; Dastoor and Larocque 2004; Presto and Granite 2006; Ahmaruzzaman 2010). Mercury contamination, especially that originating from energy production processes, still remains a significant problem that is not yet fully resolved. New restrictions in international law, such as the Minamata Convention (UNEP 2013b) requirements, as well as new BREF/BAT restrictions from the Industrial Emissions Directive (European Council 2010), require a significant reduction of anthropogenic mercury emissions. This forces researchers in both industry and science to find effective solutions for mercury control and removal. The main aim of this article is to present the state of art or latest solutions regarding mercury removal from gases and explore their potential for wider application in the energy sector. The authors main intention is to show many of the latest examples of solid sorbents applied in removal of elemental mercury from gases. Sorbents are discussed, taking into account their origins or sources and their textural properties (properties that give them a high affinity for mercury), such as specific surface area, total pore volume, volume of micropores and average pore diameter. The characteristics of sorbents are supplemented with information on the conditions under which mercury removal tests are carried out: sorbent mass, carrier gas composition, carrier gas temperature, flow rate and 10% mercury breakthrough time/experiment duration, as well as efficiency expressed as a percentage and a description of the mechanisms responsible for mercury removal. The indicated sorbents and the solutions used to modify them and increase their affinity for removing elemental mercury, have the potential for wider application.

2 Worldwide sources and emissions of mercury

Mercury sources can be divided into natural and anthropogenic. Natural sources include volcanic activity and mercury emissions from the oceans. Anthropogenic sources are mainly emissions from the combustion of fossil fuels and emissions from the processing of raw materials, as well as emissions appearing at various stages of the evolution of mercury-containing products. According to the 2010 calculations, from 5000 to 8000 Mg of mercury was emitted globally from natural and anthropogenic sources. The mercury emissions caused by human activity amounted to 1960 Mg, accounting for about 30% of all mercury released into the air. Another 10% came from natural sources, while 60% was mercury released over the centuries and accumulated in both soils and oceans. The highest mercury-emitting sector in the world is artisanal and small-scale gold mining (ASGM), which is responsible

for 35%–37% of anthropogenically produced mercury per year, or approximately 727 Mg. The mercury emissions from this sector have doubled since 2005. The next most highly emitting sectors are the energy industry, based on coal combustion processes, the production of ferrous and non-ferrous metals and the cement production sector (UNEP 2011, 2013a; EEA 2016).

3 Cycle of mercury in the energy sector, emissions and international legal restrictions

Mercury is an element naturally occurring in fossil fuels, e.g., in coals. Combustion of fossil fuels to obtain energy is still one of the main factors causing the emission of mercury compounds into the environment, mainly into the atmosphere. Mercury emitted anthropogenically can travel thousands of kilometres through air streams, before it is deposited on the ground by rainfall or through the fall of solid particles with which the mercury is bonded. In 2010, coal combustion processes were responsible for 24% of anthropogenically emitted mercury, i.e., about 475 Mg globally. The energy sector based on coal was then the second-largest industrial sector responsible for mercury emissions (the largest was artisanal and small-scale gold mining). Most of these processes take place in power plants and in combined heat and power plants. Emissions from other sources, such as homes with coal fires, were lower than expected in the previous global assessment of 2005 (UNEP 2013a). Currently, the demand of the energy sector for coal has slightly decreased, especially in European countries, and 2016 was the second year in a row where a decline in the demand for coal was recorded. The future of coal in Europe is more and more associated with such countries as Poland, Germany or the Czech Republic, which uses more than half the coal consumed in the European Union. On the other hand, the demand has increased in Asian countries. New technologies allowing the efficiency of energy production to be increased in relation to the amount of fuel consumed, the use of flue gas cleaning devices and increasingly restrictive regulations on the quality of fuels used, have in recent years reduced the mercury emissions from coal-fired power plants (UNEP 2013a; International Energy Agency 2017). The two-year decline in demand prior to 2016 was very close to the record decline in the early 1990s. Global demand for coal fell by 1.9% in 2016, to reach a level of 5357 Mt. The reduction was mainly due to low gas prices, a sharp increase in energy produced from renewable sources and an increase in the efficiency of combustion processes. In 2016, even the significant increase in coal consumption in India and some Asian countries was not able to offset huge declines in the demand for coal in countries with leading economies. The decrease in demand for coal in the US (for the third consecutive year) was mainly caused by low gas prices. In China (also for the third year in a row), the reason was lower consumption in the industrial and household sectors, related to the desire to improve air quality. In Great Britain, there was a reduction by as much as 50%, in this case the main reason was the recently introduced increased price for carbon dioxide emissions. The forecasts for 2022 anticipate a decrease in the share of coal in the global energy mix from 27% to 26%, mainly due to the low growth dynamics of the demand for this raw material in relation to other fuels. In 2022, the demand for coal will probably be concentrated mainly in India and South East Asia. On the other hand, demand for coal will fall in Europe, Canada, the United States and China. In these countries—currently the largest coal consumers—a structural slow decline is forecast, with some fluctuations associated with short-term market requirements (International Energy Agency 2017). There is a direct relationship between the amount of coal burned for the purpose of obtaining electricity and heat and the emission of mercury contained in this raw material.

3.1 Mercury in coals

Mercury occurs as an impurity in coals in trace amounts, as several different species. Most mercury species are related to sulphide minerals, mostly pyrite. Sometimes, mercury occurring with pyrite accounts for about 65%–70% of the total Hg in coal. Mercury is also related to the organic fraction in coal, as well as to other ash-forming minerals in coal. The average mercury content in coals varies globally and achieves values in the range 100 to 480 ppb (Yudovich and Ketris 2005; Park et al. 2008). According to various authors, Polish coals are characterized by a slightly different mercury content. For hard and brown coals, this varies within the range 50 to 450 ppb (Wojnar and Wisz 2006; Olkuski 2007; Burmistrz et al. 2008, 2014). This means that values are often above the global average.

According to US EPA (2002), in 14 typical coal samples mined in the United States, the mercury content was from 80 to 220 ppb. The mercury content values are as follows. For anthracite: Pennsylvania anthracite—180 ppb. For bituminous coals: Uinta—80 ppb, Raton Mesa—90 ppb, Eastern Interior—100 ppb, Western Interior—180 ppb and Appalachian—200 ppb. For sub-bituminous coals: San Juan River—80 ppb, Hams River—90 ppb, Green River—90 ppb, Powder River—90 ppb, Southwest Utah—90 ppb and Wind River—180 ppb. For lignite: Fort Union—130 ppb, Texas and Mississippi—220 ppb. In Yudovich and Ketris (2005), it was reported that in the United States over 40 Mg of mercury was emitted into the atmosphere annually, as a consequence of coal combustion.

China is recognized as the largest coal producer and consumer, as well as the highest mercury emitter in the world. By 2007, the coal consumption of the power generation sector in China increased to 1.49 billion Mg. In Wang et al. (2010), studies were performed on several samples from six typical coal-fired power plants across China. Mercury contents in the analysed coal samples were as follows: 17 ± 5, 385 ± 113, 35 ± 10, 174 ± 19, 142 ± 38 and 233 ± 12 ppb. Unfortunately, as reported in Wu et al. (2006); Pirrone et al. (2009), due to lack of information on Hg emission rates and species profiles from Chinese utility boilers, the total Hg emissions were estimated, with possible errors of approximately $-40\% \sim +70\%$.

Due to fast growth in both population and the economy, India is one of the fastest-developing countries in the world. The demand for energy grows along with rapid development. India is the third-largest producer of hard coal, after China and the US. Coal is the main source of energy in India, and around 70% of the heat and electricity production in India is from indigenous coals (Mills 2007). According to the AMAP (Arctic Monitoring and Assessment Programme) inventory of 2008, total coal consumption for India was 404.7 Mt of hard coal (anthracite and bituminous coal) and 60 Mt of soft coal (lignite and brown coal). Stationary combustion (all fuels) is by far the largest sector for mercury emissions in India, amounting to almost 140 Mg annually (AMAP 2008; Sloss 2012). Coals extracted in India are reported to be more contaminated with mercury than those of other countries. Based on a study performed on coal samples from eight Indian power plants (Kumari 2011), it was reported that the mercury content varied from 180 to 610 ppb, with a mean of 334 ppb.

According to Wojnar and Wisz (2006), results were obtained from several power plants in Poland showing the amounts of mercury introduced via fuels into the combustion processes in power plants (Table 1). The results show that the amount of mercury associated with lignite is about three times greater than for hard coal. The amounts of mercury released annually in Poland through the combustion of lignite and hard coal are 15 and 5 Mg respectively. The amount of mercury emitted into the environment is greatly affected by the mercury content of the coal being burned, the chemical composition of the coal burned (especially sulphur, chlorine, bromine, calcium and iron content), the boiler type, the processes used for exhaust gas purification and their effectiveness, mercury species in the exhaust gas leaving the boiler, the content of flammable parts (elemental of carbon) in fly ash and the content of oxidizing components in the exhaust gas (Hall et al. 1991; Galbreath and Zygarlicke 2000; Gerasimov 2005; Zhang et al. 2008).

Table 1 Mercury concentration in Polish coals according to the Central Laboratory of "Energopomiar" (Wojnar and Wisz 2006)

No.	Mercury concentration, ppb (μg/kg) Coal as received
Hard coal	
1	64–100
2	97–141
3	84–120
4	53–92
5	100–105
6	93–132
7	66–109
8	54–124
9	56–90
Bituminous coal	
1	172–283
2	117–370

3.2 Mercury in coal combustion products

Mercury occurs also in coal combustion products (CCPs). Group of CCPs include bottom ashes, slags, fly ashes, bottom sediments and gypsum generated during FGD processes. CCPs deposited in landfill pose a high risk and may be a source of mercury re-emission into the environment (Hassett et al. 1999). Preliminary studies on this were performed in Heebink and Hassett (2002). The stability of mercury in CCPs was studied. For this study, six samples of CCPs with the above-mentioned standard mercury content, were collected. Significant mercury release potential into the environment was assumed. The samples were: two fly ashes originating from the combustion of Eastern American bituminous coal with a total mercury content of 0.140 and 0.268 μg/g, two fly ashes from South African low-quality coal with a total mercury content of 0.638 and 0.555 μg/g, fly ash from Powder River Basin—sub-bituminous coal blended with petroleum coke with total mercury content of 0.112 μg/g and PRB sub-bituminous coal fly ash incorporated into flue gas desulphurization material with a total mercury content of 0.736 μg/g. A 100 g sample of each type was prepared, and then air (purified from mercury) was passed through the sample, with a flow rate of 1 mL/min. Then, the air was pumped through a gold-covered quartz trap to collect the released mercury vapour. Samples were maintained under given conditions at ambient temperature (about 37 °C) for 90 days (d). The average level of mercury release from the fly ash samples was 0.030 pg Hg/g CCBs/d. In a power plant producing around 200,000 Mg of fly ash per year, a maximum of 2 g of Hg will be released from ash during the

year. According to Heebink and Hassett (2002) and Hassett et al. (2004), investigations were developed, the next stage of which was to analyse the effect of long-term mercury release from CCPs. The fly ash used for this study came from the same sources as above, using slightly larger samples of weight 150 g. This time, the experiment lasted for 264 d and the gold-covered quartz traps were desorbed at 500 °C. The mass of released mercury was analysed using atomic fluorescence. The traps were desorbed several times, in order to extract all the absorbed mercury. The final result refers to the total amount of mercury after desorption of the traps. The results have been revised, and the amounts of mercury potentially released into the environment have been defined as of a smaller order than in the initial tests.

In case of CCPs in Poland, the mercury content was determined at similar levels as those reported in Wojnar and Wisz (2006) (Table 2). The values in the table below are from samples taken from several power plants in Poland. Considering the mercury content of the CCP, the presented results show that mercury is concentrated mainly in fly ash, where its density is many times higher than in the case of furnace slags.

On the basis of the obtained results for the mercury content of coals and CCPs, Wojnar and Wisz (2006) attempted to estimate the amount of mercury released during combustion processes. The emission value was obtained by subtraction of the amount of mercury contained in furnace wastes (in the dry state) from the amount of mercury which was delivered to the process by the coal (under working conditions). The ash content in the coal and the flammable parts of furnace wastes were taken into account in the calculations. The results are presented in the table below (Table 3). Differences in the mercury content of individual components result from different carbon sources and variable ash content (the higher the ash content, the more mercury is present). Different degrees of mercury emission may result from different types of furnace (pulverized boiler, fluidized bed boiler, grate boiler, etc.) and boiler equipment with different protective installations, such as dedusting systems (electrostatic precipitator, bag filter) and desulphurization installations in the exhaust gas route (Table 3).

Table 2 Comparison of distributions of mercury contents in Polish CCPs (Wojnar and Wisz 2006)

No.	Mercury concentration, ppb (μg/kg)	
	Slag in a dry state	Fly ash in dry state
Hard coal		
1	9–16	126–265
2	6–10	445–1000
3	2–5	372–468
4	2–11	187–476
5	4–5	374–486
6	2–5	224–229
7	5–17	318–554
8	4–11	229–539
9	13–30	378–710
Bituminous coal		
10	14–28	538–1377
11	26–89	125–521

3.3 Mercury species and their amounts and transformations in flue gases

Coal combustion in the energy sector is a complex process. During coal combustion there are many reactions leading to the decomposition and transformation of mercury-containing compounds. Mercury occurs in the flue gas via a number of thermochemical reactions. Essentially, it is transformed and released in three major forms. The first form is the vapour-phase elemental form, Hg^0. Some of the mercury may be in the form of the oxidized vapour-phase Hg^{2+}, produced via homogeneous (gas–gas) or heterogeneous (gas–solid) reactions. This form occurs primarily as $HgCl_2$. Mercury may also be bonded in a particulate matter phase—Hg^p (Gale et al. 2008; Lopez-Anton et al. 2010; Wang et al. 2010). Oxidized mercury (Hg^{2+}) is a water-soluble form and, along with particle-bonded Hg^p, may be captured by fabric filters, wet and dry flue gas desulphurization (FGD), selective catalytic reduction (SCR) or cold and hot electrostatic precipitators (ESP). These technologies are classified as conventional air pollution control devices (APCDs). Unfortunately, the elemental form of mercury is insoluble in water and very difficult to capture using APCD systems. Most of this species is released into the environment along with the flue gas (Galbreath and Zygarlicke 2000; Yang et al. 2007; Chen et al. 2008; Chmielniak et al. 2010; Wang et al. 2010).

As reported in Senior et al. (2000) and Gale et al. (2008), almost the entire coal mercury content is released into the flue gas in the elemental form during combustion over 1000 °C. This is the only stable form of mercury found in flue gas at temperatures above 600–700 °C. When the combustion temperature decreases to approximately 540 °C, some Hg^0 is oxidized to Hg^{2+}. This process is a result of the interaction of mercury with active components of flue gas, mainly with atomic Cl from HCl, Cl_2 or HOCl. The process of Hg^0 oxidation is controlled by atomic Cl cycling, which has been identified as the main mercury transformation mechanism (Niksa et al. 2001). This process, which includes homogeneous and heterogeneous

Table 3 Mercury concentration during coal combustion processes (Wojnar and Wisz 2006)

No.	Material	Ash content in dry state	Combustible parts in dry state	Mercury content			Mercury emission (ppb)	Percent of emitted mercury (%)
				As received (ppb)	Dry state (ppb)	As received of coal (μg/kg)		
1	Coal	6.4	–	226.5	–	–	204.21	90.16
	Ash	–	0.34	–	452	21.07		
	Slag	–	52.85	–	45	0.59		
2	Coal	19.7	–	90.0	–	–		37.89
	Ash	–	2.47	–	378	55.13		
	Slag	–	2.52	–	30	0.77		
3	Coal	11.3	–	64.0	–	–	50.36	78.69
	Ash	–	1.35	–	162	13.40		
	Slag	–	2.84	–	16	0.24		
4	Coal	12.2	–	47.0	–	–	20.47	43.55
	Ash	–	0.96	–	297	26.43		
	Slag	–	3.96	–	6	0.10		
5	Coal	18.0	–	183.0	–	–	105.33	57.55
	Ash	–	3.59	–	574	77.30		
	Slag	–	14.00	–	14	0.37		

reactions, is driven by the thermodynamic equilibrium but restricted by reaction kinetics (Widmer et al. 2000). Moreover, the oxidation rate is higher when the chlorine concentration in flue gas is elevated and the total mercury amount is lower (Zhang et al. 2013). The presence of NO_x and SO_x in flue gas negatively affects the oxidation process. At temperatures above 400 °C and in the presence of chlorine, a portion of the elemental mercury is oxidized to the gaseous form, $HgCl_2$. At low temperatures (100–300 °C), heterogeneous reactions on the fly ash surface start to play a more dominant role. Heterogeneous processes are responsible for the Hg^0 oxidation rate, as well as for the contribution of Hg^{2+} adsorption on fly ash particles. The result is the formation of Hg^p. During combustion processes at temperatures below 200 °C, mercury begins to be released, regardless of the form in which it occurs in the coal (Galbreath and Zygarlicke 2000; Pavlish et al. 2003; Sterling et al. 2004). In Bhardwaj et al. (2009), it was found that the specific surface area (SSA), loss on ignition (LOI) and average particle size, positively correlated with both the Hg^0 oxidation and the Hg^{2+} adsorption. In addition, the significant influence of inorganic components such as CuO, TiO_2 or Fe_2O_3 should be mentioned. According to Dunham et al. (2003) and Norton et al. (2003), these substances have a significant impact on mercury oxidation and adsorption processes. When the amount of mercury in the flue gas varies at low levels and other exhaust components do not have a negative effect, it is possible to remove the majority of mercury species simultaneously with other flue gas cleaning processes. These processes include the removal of nitrogen oxides, sulphur oxides and dust. These are the so-called passive mercury removal methods. In these cases, the mercury removal efficiency depends mainly on the mercury species and the ratio of Hg^0 to Hg^{2+}, which varies in the range 90:10–20:80. In addition, the temperature of the fumes and the efficiency of operation of individual exhaust purification nodes, influence the efficiency of mercury removal (Prestbo and Bloom 1995; Bujny et al. 2012). When the mercury content in the exhaust gases is high and the composition of the exhaust gases is unfavourable (characterized by a low content of chlorine, bromine and iron and a high calcium content), it is necessary to introduce additional technologies for mercury gas purification, i.e., the so-called active methods (Srogi 2007; Pavlish et al. 2010).

3.4 Mercury emission into the environment

Estimates indicate that in 2005, around 1930 Mg of mercury was emitted from anthropogenic sources on a global scale, of which 45% were emissions from coal combustion, 30% from gold production, 9% from metallurgy, 7% from cement plants, 6% from waste incineration plants and 3% from the production of chlorine and alkalis and from crematoria (Burmistrz et al. 2014). In UNEP (2013a), more accurate data are provided on mercury emission, for 2010. The industries in which mercury is used deliberately are recognized as the largest mercury emitters among anthropogenic sources. They were responsible for around 44% of total mercury emissions. Among these, the most important

sectors are: artisanal and small-scale gold production (410–1040 Mg, accounts for 37%), consumer product wastes (23.7–330 Mg, accounts for 5%), the chlor-alkali industry (10.2–54.7 Mg, accounts for 1%) and cremation and dental amalgam (0.9–11.9 Mg, accounts for < 1%). Another huge industry responsible for significant mercury emissions into the environment, is the energy industry, involving combustion of fossil fuels (25% of total mercury emissions), with particular emphasis on coal combustion processes (304–678 Mg, accounts for 24%) and gas and oil combustion processes (4.5–16.3 Mg, accounts for 1%). Another industry responsible for high mercury emissions is the mining, metallurgy and metal production industry (around 34% of total mercury emissions). The sectors are: primary production of ferrous metals (20–241 Mg, accounts for 2%), primary production of non-ferrous metals (82–660 Mg, accounts for 10%), large-scale gold production (0.7–247 Mg, accounts for 5%), mine production of mercury (6.9–17.8 Mg, accounts for < 1%) and cement production (65.5–646 Mg, accounts for 9%). In addition, oil refining (7.3–26.4 Mg, accounts for 1%) and contaminated sites (70–95 Mg, accounts for 4%) have a significant effect on total global mercury emissions. In UNEP (2013a), sectors are also indicated for which the amount of mercury emitted is not currently quantified but may be significant. These sectors are: biofuel production and combustion, vinyl chloride monomer production, emissions during secondary metals and ferro-alloys production, oil and gas extraction, transport and processing other than refinery emissions, industrial hazardous waste incineration and disposal, sewage sludge incineration, preparation of dental amalgam fillings and disposal of removed fillings containing mercury.

Table 4 below shows mercury emissions changes at the scale of selected European countries, compared to 1990, which is treated as 100%. In the vast majority of countries, mercury emissions into the environment have been significantly reduced. At the scale of the whole of Europe, mercury emissions decreased by 74.61% between 1990 and 2015. During the 25 analysed years, with the exception of 2010, the year-on-year decline was maintained. The energy sector of the European Union in 2015 was responsible for about 42% of anthropogenic mercury emissions (EEA 2016). The phenomenon of decreasing mercury emissions should be considered very positive, but it is still insufficient and further technological development is required to reduce emissions of mercury further and to comply with new legal restrictions.

3.5 International legal restrictions

As reported in Pirrone et al. (2009), the amount of mercury in the earth's biosphere is increasing gradually, mostly due to the highly bioaccumulative properties of this element. In order to halt this harmful phenomenon, attempts have been made to regulate the production, trade, storage and emission of mercury. To achieve this goal, a number of legal acts have been passed, starting at the global scale and ending with national laws. The most important document with a global range that concerns the problem of mercury is the Minamata Convention (UNEP 2013b). The Minamata Convention imposes restrictions on mercury extraction, trade, use in products and industrial processes and emission to the atmosphere, water and soils, and regulates waste management, methods of storage and remediation of contaminated areas. This document was adopted in January 2013 in Geneva and is presently being ratified by other countries. The Minamata Convention entered into force on 16 August 2017. According to current data, 128 countries have signed the Minamata Convention. The Polish government representative signed this document on 24th September 2014, when 71 countries had ratified the convention, five countries were at acceptance level, three countries were at the approval stage and 23 countries were at the accession level.

In the European Union, the most important legal documents (imposing restrictions on mercury emissions) from the energy industry point of view, are the Council and European Commission Directives (EU) 98/83/EC (European Commission 1998), in particular Directive (EU) 2010/75/EU of the European Parliament (European Council 2010), which was put into practice in 2016 and imposes new emission standards for SO_2, NO_x, dusts and heavy metals, including mercury. In the case of coal-fired sources, the document imposes an obligation to measure total emissions of this element annually. In 2017, the Directive was updated and now aims to introduce very strong restrictions, particularly for combustion power units where the main fuels are hard coal and lignite. Directive 2010/75/EU contains guidelines on the best available techniques (BAT) (Lecomte et al. 2017), applicable to large combustion plants. In the case of mercury emissions (in exhaust gases), the standards are set at the following levels for hard-coal-fired power plants, and they must be observed until 2021.

(1) 1–3 μg/N m^3 for new installations with power up to 300 MWt
(2) 1–9 μg/N m^3 for existing installations with power up to 300 MWt
(3) 1–2 μg/N m^3 for new installations with power above 300 MWt
(4) 1–4 μg/N m^3 for existing installations with power above 300 MWt

Table 4 Mercury emission changes and trends in European countries, 1990–2015 (EEA 2016)

Country	Emission changes in-Index (1990=100%) up to 2015 (%)	Year	Trend in mercury emission in countries mentioned beside (%)
Austria	− 54.57	1990	100
Belgium	− 80.94	1991	94.31
Bulgaria	− 67.82	1992	87.66
Croatia	− 58.44	1993	75.83
Cyprus	− 4.95	1994	72.74
Czech Republic	− 71.62	1995	70.07
Denmark	− 90.63	1996	66.12
Estonia	− 53.06	1997	62.37
Finland	− 39.75	1998	58.88
France	− 86.14	1999	64.58
Germany	− 73.90	2000	51.89
Hungary	− 64.17	2001	49.18
Iceland	518.36	2002	47.61
Ireland	− 56.39	2003	45.78
Italy	− 29.43	2004	45.05
Latvia	− 72.67	2005	43.43
Lichtenstein	10.07	2006	42.92
Lithuania	11.00	2007	41.53
Luxemburg	− 81.23	2008	39.71
Malta	− 98.78	2009	28.54
Netherlands	− 84.38	2010	28.82
Norway	− 83.25	2011	28.00
Poland	− 25.40	2012	26.92
Portugal	− 45.70	2013	26.06
Romania	− 81.40	2014	25.54
Slovakia	− 93.98	2015	25.39
Slovenia	− 51.35	2016	ND
Spain	− 64.30	2017	ND
Sweden	− 73.08	2018	ND
Switzerland	− 89.96	2019	ND
United Kingdom	− 87.29		

In the case of mercury emissions (in exhaust gases), the standards are set at the following levels for lignite-fired power plants.

(1) 1–5 μg/N m^3 for new installations with power up to 300 MWt
(2) 1–10 μg/N m^3 for existing installations with power up to 300 MWt
(3) 1–4 μg/N m^3 for new installations with power above 300 MWt
(4) 1–7 μg/N m^3 for existing installations with power above 300 MWt

In order to comply with the restrictions, further work is needed to develop techniques for exhaust gas purification. This paper helps to meet this challenge by presenting the latest proposals for sorbents capable of capturing elemental mercury and having the potential to be implemented on a larger scale.

4 Solid sorbents for mercury removal

One of the potential solutions, representing a direct method of mercury removal, is the application of solid sorbents in the flue duct. During the last few decades, scientists have tested a wide range of materials with promising features for mercury sorption. It has been found that high adsorption capability and proper oxidation ability are the two most essential properties (Zhao et al. 2017). Based on a review of the merits of mercury sorbents, it can be concluded that

the most important groups of sorbents have emerged recently. These are activated carbons and metal oxides (Sjostrom et al. 2010; Tan et al. 2012; Gao et al. 2013). Main justification for selection of sorbents was application for the purpose of removing mercury from gases confirmed by literature review, topicality of data and reputation of the journal where study was published. The most important and promising solid sorbents from a wider spectrum of materials are discussed below.

4.1 Activated carbons

Activated carbons (AC) are relatively popular and universal sorbents. Various methods of AC production and functionalization for various processes have been widely discussed in the literature, including the factors that have the greatest impact on the product obtained, its surface and textural properties and other properties related to the removal of elemental mercury. These factors include, among others, heating speed, maximum process temperature, pressure, contact time with steam, moisture, etc. (Manyà 2012; Shewchuk et al. 2016). A tremendous advantage of AC materials is that they can be obtained from a wide range of materials which may be either natural or synthetic, e.g., eucalyptus wood (Silva et al. 2010) or peat (Khadiran et al. 2015). It is worth mentioning that they can also be obtained from some industrial waste materials, e.g., olive-waste cakes (Baçaoui et al. 2001), biomass materials (Amaya et al. 2007), coir pith (Namasivayam and Sangeetha 2006), waste coffee (Kemp et al. 2015), peanut shells (Eldien et al. 2016), rice husks (Le Van and Luong Thi 2014), the sago industry (Kadirvelu et al. 2004) or tyre-waste thermolysis char (López et al. 2013). Unfortunately AC application, especially on a large scale, is limited, due to high cost or complicated preparation and regeneration processes (Xu et al. 2012). The properties of a given activated carbon depend on the physico-chemical characteristics of the precursors and the activation methods used (physical or chemical). Physical activation consists of subjecting carbonaceous materials to carbonization processes at temperatures ranging from 500 to 900 °C. This process takes place in an inert atmosphere, followed by proper activation through the use of substances such as CO_2 or water vapour. In the case of chemical activation, the raw carbonaceous material is impregnated with chemical compounds such as $ZnCl_2$, H_3PO_4 or KOH, and then heated in an inert atmosphere. Chemical activation is the preferred method, due to the higher efficiency achieved, the use of lower temperatures, shorter activation times, the overall simplicity of the mechanisms and the possibility of obtaining structures with a relatively high specific surface area. The most important features of active carbons leading to their wide usability include surface area, bulk density and chemical characteristics represented by pH, ash content and conductivity. The developed specific surface area and the structure of micropores increase the affinity of AC for mercury removal (Guo and Rockstraw 2007; Demiral et al. 2008; Ahmed and Theydan 2012). Supplementary material 1 presents the characteristics of activated carbons used recently for elemental mercury removal experiments. Supplementary material 2 shows the experimental parameters, as well as the mechanisms responsible for mercury capture, as proposed by the cited papers' authors (ordinal numbers from the first column refer to the same samples in both Supplementary material 1 and 2).

In Rodríguez-Pérez et al. (2011), the well-known phenomenon of amalgamation of mercury with precious metal is exploited (Brown et al. 1999). In this case, the metal that increases the sorbent's affinity for binding to mercury, is gold. The phenomenon of the amalgamation of mercury and gold is well known and has been widely described in the literature (Fiałkowski et al. 2004; Veiga et al. 2006; Hou et al. 2015). The starting material is the commercially available activated carbon Norit RB3. To obtain increased selectivity and effectiveness in capturing mercury, the material was impregnated with gold nanoparticles. Two methods of impregnation were used, for comparison. In the first case, gold impregnation was carried out in polyvinyl alcohol (PVA), while the second impregnation environment was tetrakis (hydroxymethyl) phosphonium chloride (THPC). THPC-impregnated carbons proved to be more effective in mercury removal processes, although they were characterized by very similar retention capacity values. Different concentrations of gold that functionalized AC for Hg removal were also analysed and compared (gold dripping: 0.05 wt%, 0.1 wt%, 0.5 wt% and 1 wt%). The activated sorbents are characterized by a relatively high specific surface area (ranging from 1139 to 1166 m^2/g), total pore volume and volume of micropores. In the mercury removal experiment, 0.08 g of a given sorbent was subjected to testing. The carrier gas was a mixture of oxygen and nitrogen and the flow was set at 0.5 L/min. The initial concentration of mercury in the carrier gas was set at 100 $\mu g/m^3$ and the process temperature was 120 °C. The experiment time was set to 4320 min. Samples obtained using the PVA method, dropped with 0.05 wt%, 0.1 wt%, 0.5 wt% and 1 wt% of Au, achieved mercury removal efficiencies of 30%, 70%, 60% and 65% respectively. Samples obtained using the THPC method, dropped with 0.05 wt%, 0.1 wt%, 0.5 wt% and 1 wt% of Au, achieved mercury removal efficiencies of 50%, 82%, 67% and 60% respectively. The sample RB3 THPC0.1 achieved 82% mercury removal efficiency, which is a very good result, given the low weight of the sorbent used and the relatively high initial concentration of elemental mercury in the carrier gas. The authors point to amalgamations of mercury

and gold as the main mechanisms for mercury binding in the sorbent. The disadvantage of the proposed solution is likely to be the cost of the activating substance—gold nanoparticles.

In Fan et al. (2010), commercially available activated carbon (purchased from Jiangsu Sutong Carbon Fiber Co., Ltd.) was impregnated with cerium oxide. The amount of activating substance was in the range 2 wt%–15 wt%. The obtained sorbents were also characterized by relatively high values of the specific surface area (from 965.3 to 1589.5 m^2/g) and total pore volume (from 0.51 to 0.87 cm^3/g). The average pore diameter varied between 1.3 and 1.9 nm. The above values are arranged almost linearly with a specific trend—the highest values characterize raw carbon ACF assets and the lowest ones refer to the sample 15% CeO_2/ACF. This indicates the impact of the impregnation process on the decrease in the values of textural features. In the mercury removal experiments, 0.1 g of the obtained sorbent was used. The carrier gas was a mixture of O_2, N_2, NO, CO_2 and SO_2 and the flow rate was set to 1 L/min. The experiment was carried out at 150 °C and the test time was set to 200 min. The initial mercury concentration was set to 20 $\mu g/m^3$. The obtained sorbents achieved a mercury removal efficiency in the range of about 60% to 90%. The highest efficiency of mercury removal (about 90%) was achieved by the sample 6% CeO_2/ACF (with textural properties of S_{BET}: 1275.4 g/m^2, total pore volume: 0.68 cm^3/g and average pore diameter: 1.5 nm). Except in the examination of the loading values effect, (Fan et al. 2010) also tested the effect of the calcination temperature of the samples on mercury removal efficiency (at 300, 400 and 500 °C), the effect of temperature on the removal process (at 90, 120, 150, 180 and 210 °C), the effect of NO content in the carrier gas (0, 400 and 800 ppm) and the effect of SO_2 content in the carrier gas (0–1000 ppm). Studies confirm that functionalization with cerium oxides increases AC affinity for mercury removal by generating multiple functional groups.

In Wang et al. (2016), functionalization of AC was performed via the equivalent-volume impregnation method, using various amounts of $Ce(NO_3)_3{\cdot}6H_2O$ and $Fe(NO_3)_3{\cdot}9H_2O$. The starting material was purchased from Inner Mongolia's Kexing Carbon Co., Ltd. (columnar granules with a length of 7-9 mm and an average diameter of 5 mm). In contrast to previous studies, the ACs in this case are characterized by lower values of the specific surface area (varying from 271.6 to 329.6 m^2/g) and total pore volume (from 0.13 to 0.16 cm^3/g). Average pore diameters reached slightly higher values, compared to their predecessors (from 1.9 to 2.01 nm). In this case, no linear dependence of the variability of the textural features was observed with respect to the amount of activating substances used. For the mercury removal experiments, an optimized sorbent dose was used (the authors did not give the exact value in the paper). The gas carrier was a mixture of N_2, NO, SO_2 and CO_2, and the flow rate was set to 1 L/min. The experiment examining the influence of the amount of activating substance on the efficiency of elemental mercury removal was carried out at 110 °C, over a time period of 180 min. The initial mercury concentration in the gas carrier was set to about 70 $\mu g/m^3$. The obtained sorbents achieved a mercury removal efficiency in the range of about 40% to approximately 90%. The highest result (89.29%) was obtained by the Fe_3Ce_3/AC sample, where the mass ratio of Fe_2O_3 and CeO_2 was 3:3 and the total mass percentage of Fe–Ce mixed oxides was 6%. In addition to studying the optimal mass ratio of Fe_2O_3 and CeO_2 on the Hg^0 removal efficiency, the authors also considered the optimal temperature of the mercury removal process (50–200 °C). The effect of the content of individual carrier gas components, such as O_2, NO and SO_2, was also studied. The authors pointed out that the removal of mercury in this case corresponds to mechanisms related to adsorption and oxidation. Lattice oxygen, chemisorbed oxygen and/or weakly bonded oxygen species all make a contribution to Hg^0 oxidation. The use of iron and cerium oxides seems to be a favourable and reasonable solution, from an economic point of view.

Another example of the use of cerium compounds for the modification of activated carbons to increase their mercury affinity, is given in Wu et al. (2017). Commercially available activated carbon purchased from Shanghai Xinhui Activated Carbon Co., Ltd. was subjected to functionalization with cerium oxide. In some cases, the functionalization was extended to the use of manganese compounds. The loading of CeO_2 ranged from 1 wt% to 7 wt% (1%, 3%, 5% and 7%), and the mass ratio of manganese to cerium was 0.7. The S_{BET} changed with the amount of activating substance used. For raw AC it was 673.4 m^2/g. For the sample activated with 1% CeO_2, the S_{BET} slightly increased to 687 m^2/g. With increasing amounts of CeO_2, e.g., 3 wt%, 5 wt% and 7 wt%, the specific surface area decreased by 655.1, 629.1 and 606.1 m^2/g. A slight decrease was also recorded in the total pore volume values (from 0.37 to 0.33 cm^3/g) and the micropore volume values (from 0.20 to 0.18 cm^3/g). Average pore diameter was maintained at a stable value of 2.19–2.20 nm. Analogous trends were observed for samples additionally modified with manganese. The simultaneous use of cerium oxide and manganese resulted in further reductions: the values of S_{BET} decreased (from 676.8 m^2/g for the sample 1% CeO_2–Mn(0.7)/AC up to 525.9 m^2/g for the sample 7% CeO_2–Mn(0.7)/AC), the total pore volume decreased (from 0.37 cm^3/g for the sample 1% CeO_2–Mn(0.7)/AC up to 0.28 cm^3/g for the sample 7% CeO_2–Mn(0.7)/AC) and the micropore volume decreased (from 0.20 cm^3/g for the

sample 1% CeO_2–Mn(0.7)/AC up to 0.15 cm^3/g for the sample 7% CeO_2–Mn(0.7)/AC). The average pore diameter decreased from 2.20 nm for the sample 1% CeO_2–Mn(0.7)/AC to 2.17 nm for the sample 7% CeO_2–Mn(0.7)/AC. In the mercury removal experiments, 0.1 g of a given sorbent and 1 g of quartz sand were used. The medium for mercury was an artificially produced gas corresponding to the conditions of the real flue gas. The flow rate was set to 1.5 L/min, while the temperature of the process was 119.85 °C. The initial mercury concentration was 40 $\mu g/m^3$ and the time of the experiment was set to 180 min. Only samples after functionalization were subjected to mercury removal tests. The mercury removal efficiency varied between 52% and 90%, with the highest result being achieved by the sample 3% CeO_2–Mn(0.7)/AC. The mechanism of mercury capture was bonding in the presence of CeO_2 and MnO_x, where Ce^{4+} and Mn^{4+} released lattice oxygen and promoted Hg^0 oxidation.

Manganese and cerium were also used in Xie et al. (2015). AC purchased from Inner Mongolia's Kexing Carbon Co., Ltd., was functionalized. The mass ratio of Mn:Ce was set to 1:1 in all the samples. Moreover, Mn-Ce mixed oxides in the MnCe/AC samples were at levels of 2 wt%, 4 wt%, 6 wt%, 8 wt% and 10 wt%, denoted MnCex/AC, where x represents the MnCe percentage of the sample. For comparison, AC was also separately exposed to manganese and cerium activation. The impregnation method was applied for the functionalization of activated carbons. The raw AC was characterized with an S_{BET} value of 366 m^2/g, a total pore volume of 0.17 cm^3/g and an average pore diameter of 1.86 nm. Most of the samples had better textural properties after functionalization, compared with raw AC, with the exception of the last sample with the activating substance with highest saturation—MnCe10/AC (which was the opposite of the previous cases). At the same time, a trend of decreasing values of textural properties with increasing amounts of activating substances, was reported. This is probably due to blockage of the pores. The highest value of S_{BET} was achieved by the sample MnCe2/AC, at 468.4 m^2/g. The total pore volume and average pore diameter for this sample were 0.22 cm^3/g and 1.88 nm respectively. The weakest result in terms of textural properties was for the sample MnCe10/AC, where the S_{BET} was 280.1 m^2/g while the total pore volume and average pore diameter values were 0.13 cm^3/g and 1.89 nm respectively. In the mercury removal experiments, 18 g of a given sorbent sample was used. The gas carrier was a mixture of N_2 and O_2 and the gas flow was set to 1 L/min. The temperature of the removal process was 190 °C and the initial Hg^0 concentration was set to 80 $\mu g/m^3$. The experiment time was set to 180 min. With the exception of raw AC (52%), very promising results for mercury removal efficiency were achieved. The next samples, i.e., MnCe2/4/6/8/10/AC, achieved 89%, 92%, 93%, 91% and 90% efficiency respectively. However, it is necessary to bear in mind the much larger mass of sorbent used, compared to previous studies. In Xie et al. (2015), the effect of varying the temperature of mercury removal processes on the mercury removal efficiency was examined by conducting tests in the temperature range from 100 to 250 °C. The influence of the content of individual carrier gas components, such as O_2, SO_2, NO and H_2O, was also studied. Among the mechanisms responsible for the removal of mercury, the authors indicated a combination of adsorption and oxidation, and both the lattice oxygen and the OH groups in MnCe6/AC contributed to Hg^0 oxidation.

The last example of the use of activated carbons to remove Hg^0 is Chen et al. (2018b), in which commercially available AC purchased from Gongyi Zhongya Purifying Water Materials Co., Ltd., was activated with cobalt and cerium compounds. For modification, the impregnation method with cobalt nitrate ($Co(NO_3)_2{\cdot}6H2O$) and $M(NO_3)x{\cdot}yH_2O$ was used (M = cerium). The analysed ACs had much lower (in comparison to their precursors) values of textural properties. The S_{BET} values varied from 62.4 m^2/g for sample Co_8Ce_3/ACs to 66 m^2/g for raw AC. The total pore volume in these studies was quite stable, varying between 0.10 and 0.11 cm^3/g. The average pore diameter had significantly higher values than in other analysed studies, in the range from 6.13 nm for the sample Ce_8/ACs to 6.82 nm for the sample Co_8/ACs. For the mercury removal experiments, 20 g of a given sorbent sample was used. The gas carrier was a mixture of HCHO, O_2 and N_2, and the flow rate varied from 0.5 to 1 L/min. The experiments were carried out over a wide temperatures range between 110 and 310 °C. The initial concentration of mercury was 90 $\mu g/m^3$ and the experiment time was set at 4000 min. The mercury removal efficiency varied between 38% for raw AC and about 70% for the sample Co_8Ce_3/ACs. Further tests in Chen et al. (2018b) also investigated the effect of the presence of HCHO on the mercury removal efficiency, as well as the effect of the content of the individual components of the carrier gas (O_2, NO, SO_2 and H_2O). The stabilities of the obtained materials were also considered. Catalytic oxidation was identified as the main mechanism responsible for elemental mercury capture.

4.2 Biochars

Biochars are stable solid charcoals obtained through carbonization, which is also a slow pyrolysis process. Biomass materials are subjected to heating in an oxygen-free or oxygen-limited environment, resulting in thermal decomposition. Typical temperatures for biochar production vary from 400 to 600 °C (Yi et al. 2017). Supplementary

material 3 presents the characteristics of biochars used recently for elemental mercury removal experiments. Supplementary material 4 gives experimental parameters as well as the mechanisms responsible for mercury capture proposed by the cited papers' authors (ordinal numbers from the first column refer to the same samples in both Supplementary material 3 and 4).

In Liu et al. (2018), the authors attempted to use the resources of oceanic biomass in the form of seaweed, to create sorbents capable of capturing elemental mercury from gas. Two types of seaweeds were subjected to a pyrolysis process, leading to the creation of biochars: Sargassum and Enteromorpha, obtained from Weihai in Shandong Province, China. The obtained materials were impregnated with potassium halides (KCl, KBr and KI—see Supplementary material 3 and 4 for an example of impregnation with KI) using 0.5 wt%, 3 wt% and 9 wt% of activating substance respectively. The authors state that in previous studies, they found that a pyrolysis temperature of 800 °C allowed much better pore structures and spacing to be obtained than is the case for pyrolysis at 400 °C or 600 °C. Pyrolysis was carried out in an N_2 atmosphere with a heating rate of 20 °C/min. After the set temperature of 800 °C was reached, it was maintained for 20 min. Sargassum and Enteromorpha biochars obtained as a result of the above process were named S800 and E800. The analysed materials are characterized by relatively low textural values. The S_{BET} value for Sargassum biochars varied between 26.2 m^2/g (for raw char) to barely 7 m^2/g (for the sample activated with 9 wt% of KI). The specific surface area decreases with the amount of halide used for activation. The highest value of total pore volume was obtained for Sargassum biochar activated using 0.5 wt% of KI. This correlates also with the lowest average pore diameter value achieved by this sample, i.e., 3.42 nm. Biochars obtained from Enteromorpha have lower surface area values. In this case S_{BET} varies between 11.2 m^2/g (for raw char) and 7.9 m^2/g (for the sample activated with 9 wt% of KI). Thus, the same trend is observed as for the Sargassum biochars. In addition, the total pore volumes achieved are comparable to the previous type of seaweed. In turn, the average pore diameter is characterized by higher values, from 12.61 to 16.72 nm. In mercury removal experiments testing the effect of using different amounts of halides to activate the biochars, 0.08 g of a given biochar sample and 0.92 of quartz sand were used. The gas carrier was a mixture of O_2, NO, SO_2, H_2O and N_2. The flow rate was set to 0.85 L/min. and the process temperature was 80°C. The initial concentration of Hg^0 was set to about 60 $\mu g/m^3$. The experiment time was 80 min. The mercury removal efficiency ranged from about 25% to about 90%. The lowest values ($\sim$25% and $\sim$35%) were obtained with raw chars. In both cases, i.e., Sargassum- and Enteromorpha-derived biochars, the highest mercury removal results were obtained with the samples activated with 3 wt% of KI, giving $\sim$90% and $\sim$85% efficiency respectively. In Liu et al. (2018), tests were also conducted on the influence of temperature changes (80, 120 and 160 °C) on mercury removal efficiency. Sorbents activated with other halides (KBr and KCl) were also analysed in further work. The impact of the content of O_2, NO, SO_2 and H_2O was also examined. The authors indicate adsorption processes as the main mechanism responsible for binding mercury. The use of widely available oceanic biomass means that the production of the above sorbents could be effective from an economic point of view.

In Yang et al. (2018b), a similar case was described, using oceanic biomass to produce biochars. The raw material used in this work was Sargassum seaweed obtained from Weihai in Shandong Province, China. Sargassum chars were obtained as a result of the pyrolysis process, which was carried out in atmosphere of nitrogen at three temperatures: 400, 600 and 800 °C. Chars were denoted as S4, S6 and S8 respectively. As the most satisfactory result was obtained for the S8 sample, it was impregnated with NH_4Br and subjected to further mercury removal tests. Raw biochars obtained at temperatures of 400 °C and 600 °C possess very poorly developed textural properties. S_{BET}, total pore volume and average pore diameter values were 1.95 and 3.71 m^2/g, 0.003 cm^3/g and 16.78 and 23.57 nm respectively. Only the S8 sample obtained at 800 °C showed better and more rewarding properties. S_{BET}, total pore volume and average pore diameter values were 26.20 m^2/g, 0.03 cm^3/g and 4.63 nm respectively. Sample S8 was subjected to impregnation with NH_4Br using 1 wt%, 5 wt% and 9 wt% of activating substance. Functionalized samples (named S8Br1, S8Br5 and S8Br9), were characterized by S_{BET} values of 20.21, 19.66 and 19.47 m^2/g respectively. The total pore volume value for all activated samples was 0.03 cm^3/g, while the average pore diameter values were 9.82, 8.98 and 10.22 nm respectively. Increasing the amount of NH_4Br caused a decrease in S_{BET} and total pore volume values, with a simultaneous increase in average pore diameter values. This can be explained by the clogging of micropores. In the mercury removal experiment aimed at indicating the optimal amount of NH_4Br, 0.25 g of the selected char sample and 1.5 g of quartz sand were used. The gas carrier was a mixture of O_2, NO, SO_2, H_2O and N_2. The flow rate was set at 0.9 L/min. The temperature of the process was 120°C and the initial Hg^0 concentration was 60 $\mu g/m^3$. The time for the experiment was 70 min. As expected, raw samples (S4, S6 and S8) were characterized by lower efficiencies, achieving 12%, 14% and 29% respectively. Activated samples (S8Br1, S8Br5 and S8Br9) achieved much better results. The mercury removal efficiency was 78.13%,

91.58% and 98.07% respectively. An increase in Hg^0 removal efficiency was observed with an increase in NH_4Br from 1 wt% to 9 wt%. In further work in Yang et al. (2018b), the temperature effect of the reaction on mercury removal efficiency was investigated by testing the obtained sorbents at 80 °C and 160 °C. As in previous cases, the influence of individual components (O_2, NO, SO_2 and H_2O) of the carrier gas was also examined. Among the mechanisms responsible for the removal of mercury, the authors indicate the adsorption and production of $HgBr_2$.

In Xu et al. (2018b), waste from rice production, i.e., rice straw, was used, from which biochars were obtained via pyrolysis. Rice straw was collected from Xuzhou in Jiangsu Province in China. This is a type of waste often used in pyrolysis processes. In this case, 2 g of dried and sieved (< 300 μm) rice straw was subjected to the pyrolysis process at a temperature of 600°C, in an atmosphere of nitrogen for 20 min. Rice straw char was modified by Cu–Ce mixed oxides, using an ultrasound-assisted impregnation method. It has been demonstrated that copper oxides show high catalytic activity and stability in mercury oxidation processes at low temperatures, increasing the sorbents' ability to remove Hg^0 (Yamaguchi et al. 2008) (Xu et al. 2014). During impregnation, different amounts of cerium nitrate (hexahydrate, AR, Xilong Scientific Co., Ltd.) and copper nitrate (trihydrate, AR, Xilong Scientific Co., Ltd.) were used. The calcination temperature was 260 °C. The samples were designated CuCe$\chi(\gamma)$/RSU(t), where χ represents the total molar concentration (mol/L) of copper nitrate and cerium nitrate in the solution resulting from the impregnation procedure, γ represents the molar ratio of Cu to Ce and U denotes ultrasound. The S_{BET} of RS char was 26.66 m^2/g, the total pore volume reached a value of 0.12 cm^3/g, the micropore volume was 0.006 cm^3/g and the average pore diameter was 18.08 nm. In the sample activated using 0.18 mol/L of copper nitrate and cerium nitrate, the S_{BET}, total pore volume, micropore volume and average pore diameter values were 28.81 m^2/g, 0.12 cm^3/g, 0.007 cm^3/g and 17.18 nm. When ultrasound assistance was used, these values were 33.79 m^2/g, 0.07 cm^3/g, 0.018 cm^3/g and 8.62 nm respectively. As can be seen, the use of ultrasound caused a slight increase in the specific surface area and a decrease in the total pore volume, while simultaneously causing an increase in the number of micropores and more than doubling the average pore diameter. In the elemental mercury removal experiment, 0.3 g of each of the rice straw char samples (RS, CuCe0.18(1/5)/RS(240) and CuCe0.18(1/5)/RSU(240)) and 4 g of quartz sand were used. The carrier gas was a mixture of N_2, O_2, SO_2 and NO and the gas flow was set to 0.8 L/min. The temperature of the removal process was set to 130 °C and the initial mercury concentration was 50 $\mu g/m^3$. The time of the experiment was set to 80 min. The effectiveness of elemental mercury removal by raw RS char was 8.60%. For the sample Ce0.18(1/5)/RS(240) this increased to 32.01% and for the sample CuCe0.18(1/5)/RSU(240) it reached 67.45%. In this case, the authors identified the main mechanisms affecting the binding of Hg^0 as oxidation and chemical adsorption. The authors also tested other values of Cu:Ce molar ratio (1:1 and 1:3) and other loading values (0, 0.06, 0.12, 0.24 and 0.30). Tests were also carried out at different temperatures (110 °C, 150 °C and 170 °C). The next analysed variable was calcination temperature after impregnation (200, 220, 240, 280 and 300 °C). In Xu et al. (2018b), the impacts of individual components of the carrier gas (N_2, O_2, SO_2, NO and H_2O) were also analysed. As in the previous case, it is also worth considering the possible economic efficiency, which is favourable as a result of the use of waste material as the main substrate and the possibility of regenerating and reusing the sorbent. Therefore, there may be wider interest in this product for this application.

An interesting study described the use of a wide variety of types of biomass waste as raw material (Wang et al. 2018). For production of biochars, the following materials were used: rice straw (R6), tobacco straw (T6), corn straw (C6), wheat straw (W6), millet straw (M6) and black bean straw (B6). The pyrolysis process was conducted in an atmosphere of pure nitrogen at a temperature of 600 °C. The biomass samples (10 g) were first rinsed in deionized water, dried and then sieved to 100–200 μm. For biochar functionalization through increasing the number of active Cl sites, the chlorine (Cl) non-thermal plasma method was used. The surface areas of biochars before activation varied between 6.3 m^2/g for black bean straw biochar and 63.8 m^2/g for millet straw biochar (M6 > R6 > W6 > C6 > T6 > B6). In the activated analogues, S_{BET} varied between 6.1 m^2/g for black bean straw biochar and 33.5 m^2/g for rice straw biochar (R6 > M6 > C6 > W6 > T6 > B6). Plasma increased the specific surface area of R6, C6 and W6, but decreased that of T6, M6 and B6. Unfortunately, the authors do not give the values of other key textural parameters. In the mercury removal experiment, 0.05 g of a given sorbent was used. The carrier gas was compressed air and the flow rate was 2 L/min. The temperature of the process was set to 150 °C and the experiment time was 90 min. Initial Hg^0 concentration was 20 $\mu g/m^3$. Raw sorbents showed zero or very low (maximum ~ 2.5%) mercury removal efficiency. The situation was slightly better for their counterparts after activation. The best result (55.8%) was obtained from sample T6Cl, followed by 35% (R6Cl), 35% (M6Cl), 20% (W6Cl), 15% (C6Cl) and 0–1% (B6Cl). Activation of the T6 sample resulted in a 36-fold increase in the adsorptive capacity. This indicates that the proposed activation procedure could be an effective way to increase the sorption capacity of some materials. It can be

concluded that Cl_2 plasma modification increases the number of Cl groups on the biochar surface, and that these Cl groups serve as activated sites that increase the Hg^0 removal efficiency.

The last example of the use of biochars to remove Hg^0 is in Yi et al. (2018). In this case, cones were used as the starting material for the production of chars. The material was rinsed in deionized water, dried and sieved to 80–100 μm. The pyrolysis was carried out at a temperature of 500 °C for 90 min., with a heating rate of 5 °C/min. The atmosphere of the pyrolysis process was pure nitrogen. The next stage was a 24 h impregnation of biochars in 30% H_2O_2 (1 g of biochar per 10 ml of solution). Solutions of $Mn(NO_3)_2$ and/or $Cu(NO_3)_2{\cdot}3H_2O$ were used for further impregnation of the materials. After impregnation was complete, the samples were heated for 4 h at 500 °C under a nitrogen atmosphere. The obtained samples were designated ACuxMny/HBC, where x and y refer to the Cu:Mn molar ratio (x:y = 3:1, 2:1, 1:1, 1:2, 1:3, 1:4 and 1:5) and a stands for the total metal oxide mass percentage in the samples (HBC + total metal oxides mass). The obtained biochars were characterized by significantly better textural properties, compared to materials in the above studies. After impregnation with H_2O_2, the sample was characterized. The S_{BET} was 178.23 m^2/g, the total pore volume was 0.09 cm^3/g and the average pore diameter was 1.4 nm. Further activation with Cu/Mn compounds caused further improvement in the textural properties. The S_{BET} for all activated samples varied between 307.13 and 320.98 m^2/g, the total pore diameter varied from 0.14 to 0.16 cm^3/g and the average pore diameter varied from 1.8 to 2.02 nm.

The use of biomass waste for the production of high-performance mercury sorbents seems to be a very good idea from an economic point of view, due to the low cost of substrates. After the development of the technology, there may be opportunities for wider application.

4.3 Zeolites

Zeolites are well-understood and well-studied materials. They possess a number of important properties: ion exchange, adsorption and molecular sieve or catalytic properties (Ahmaruzzaman 2010). These features are consequences of the characteristic crystallochemical structure. Zeolite crystal structure results from spatial bonding of SiO_4 and AlO_4 tetrahedra, which are called primary building units (PBU). These tetrahedra form larger systems through bonding with oxygen bridges, i.e., secondary building units (SBU). Within the SBU, different types of rings occur. Connection of SBU units with free corners results in characteristic channels and chambers, called cavities (Baerlocher et al. 2007; Handke 2008). Both natural and synthetic zeolites are widely applied in environmental protection technologies (Franus et al. 2015; Ospanov et al. 2016). The great advantage of zeolites is the fact that they can be synthesized from a wide range of materials containing silica and aluminium. There are many studies describing different types of substrates and synthesis methods. In Boycheva et al. (2014), Franus et al. (2014), Wdowin et al. (2014a), Czarna et al. (2016), Kunecki et al. (2017, 2018) and Panek et al. (2017), the possibility is discussed of synthesizing zeolites from fly ashes, which are by-products of hard coal and lignite combustion in the energy sector. There are also many examples of materials used as the main substrates in the synthesis of zeolites, such as natural minerals, e.g., kaolinite (Holmes et al. 2011; Johnson and Arshad 2014), pumice (Burriesci et al. 1983), obsidian (Ríos et al. 2012), diatomite (Garcia et al. 2016) and diatomaceous earth (Aguilar-Mamani et al. 2014), and some waste materials, e.g., perlite (Pichór et al. 2015), rice husk fly (Mohamed 2008, 2015) and discarded electronic devices (Tsujiguchi et al. 2014).

Pioneering work on the use of zeolites for the removal of elemental mercury has been conducted since the 1990s and is described in Morency et al. (2000) and Panagiotou et al. (2000). These authors stimulated greater interest in the attempt to use zeolites as Hg^0 sorbents. The following examples show the achievements of recent years in this area. Supplementary material 5 presents the characteristics of zeolites used recently for elemental mercury removal experiments. Supplementary material 6 shows the experimental parameters as well as the mechanisms responsible for mercury capture, proposed by the cited papers' authors (ordinal numbers from the first column refer to the same samples in both Supplementary material 5 and 6).

In Qi et al. (2015), an interesting idea is presented for removing elemental mercury using three different zeolites: Na-A, Na-X and HZSM-5. The zeolites Na-A and Na-X were purchased from Sinopharm Chemical Reagent Co., Ltd., while the zeolite HZSM-5 was purchased from Nanjing JCNANO Tech. Co., Ltd., China. Zeolites were subjected to modification with $FeCl_3$ to produce active chloride species on the surface of the samples. Zeolite functionalization was performed with iron chloride aqueous solution by an impregnation method, in proportions corresponding to different loading values. The obtained sorbents were dried, milled and sieved to 60–80 μm. XRD analysis showed a significant decrease in the crystallinity of sorbents after the modification process. In addition, NaCl crystallization caused by the ion exchange properties of zeolites affected the reduction of active chloride species production on the surface of the samples. The specific surface area of the LTA zeolite increased from 24.5 to 44.6 m^2/g in comparison to the value before activation. The total pore volume remained stable at 0.12 cm^3/g. In the case of

the FAU type of zeolite, activation with iron chloride caused a significant decrease in both S_{BET} and total pore volume values. These values decreased from 632.9 to 149.8 m^2/g and from 0.40 to 0.24 cm^3/g. For the HZMS-5 zeolite, there was also a decrease in textural properties, but to a lesser extent than for Na-X. For HZSM-5, the reported decrease in the S_{BET} value was from 405.3 to 358.9 m^2/g. The total pore volume remained stable at a level of 0.23 cm^3/g. For the removal of elemental mercury experiments, 0.05 g samples of the sorbents after activation were used. The carrier gas was pure nitrogen and the gas flow was set to 1 L/min. The process temperature was 120 °C and the initial Hg^0 concentration was 40.7 ± 0.3 $\mu g/m^3$. The time of the experiment was 180 min. The lowest mercury removal efficiency (5%) was reported for sample 5% $FeCl_3$–NaA. A removal efficiency of about 50% was achieved for sample 5% $FeCl_3$–NaX, while the highest result of up to 98% was obtained for the sample 5% $FeCl_3$-HZSM-5. The authors indicated that adsorption processes and bonding of mercury with Cl species were the main Hg^0 removal mechanisms.

Another example of the use of zeolites to remove mercury is given in Sun et al. (2018). Na-A zeolite synthesized in the laboratory underwent functionalization with silver nanoparticles. The raw Na-A zeolite had an S_{BET} value of 449.9 m^2/g and a total pore volume of 0.16 cm^3/g, with an average pore diameter of 0.45 nm. The zeolite C-AgNPs/4A was characterized by a slightly lower value of S_{BET} (in comparison to the raw zeolite) of 402.5 m^2/g. The value of the total pore volume also decreased to 0.14 cm^3/g. The average pore diameter remained at the same value of 0.45 nm. For the mercury removal experiment, 1 g of sorbent was used. The carrier gas was natural gas (CH_4) and the flow rate was set to 0.7 L/min. The process temperature was 30 °C. The mercury concentration in natural gas typically varies from 1 to 200 Mg/m^3 (Ryzhov et al. 2003). The authors did not give the exact mercury concentration in the experiment, but it should be expected to be in the given range. The experiment time was set to 200 min. The raw Na-A zeolite sample achieved about 20% mercury removal efficiency. The sample that was activated with silver nanoparticles achieved a much higher result—in the range 92%–95%. The authors pointed to the phenomenon of amalgamation as the main mechanism for mercury binding.

A very interesting solution was proposed in Cao et al. (2017). The authors created a magnetically responsive catalytic sorbent for simultaneous removal of Hg^0 and NO, intended for use in power plants. For these tests, the starting material was zeolite HZSM-5, which was modified with magnetite (Fe_3O_4), silver nanoparticles and V_2O_5, enhancing the catalytic reactivity. The obtained sorbents achieved very promising results for the simultaneous removal of elemental mercury and nitrogen oxides. The best textural properties were obtained from raw HZSM-5 zeolite. The S_{BET} was 353 m^2/g and the total pore volume was 0.20 cm^3/g. The subsequent stages of activation resulted in a decrease in textural property values. For subsequent samples the S_{BET} and total pore volume values were as follows: MagH (259 m^2/g and 0.19 cm^3/g), MagH-Ag^0 (253 m^2/g and 0.16 cm^3/g), MagH-V4 (249 m^2/g and 0.16 cm^3/g), MagH-V4-Ag^0 (237 m^2/g and 0.15 cm^3/g), MagH-V8 (230 m^2/g and 0.15 cm^3/g) and MagH-V8-Ag^0 (217 m^2/g and 0.14 cm^3/g). In the simultaneous mercury and NO removal experiment, 0.03 g of a given sorbent was used (except in the case of raw HZSM-5). The gas carrier was a mixture of O_2, CO_2, NO, NH_3, SO_2 and HCl. The flow rate was set to 0.5 L/min. The temperature of the process was 150 °C and the initial Hg^0 concentration was 79 $\mu g/m^3$. The time of the experiment was set to 180 min. The samples achieved the following removal efficiencies for Hg^0: MagH—about 12%, MagH-Ag^0—about 30%, MagH-V4—about 42%, MagH-V4-Ag^0—about 96%, MagH-V8—about 96% and MagH-V8-Ag^0—about 97%. The results of the last three samples in particular are very promising—they ensure the almost complete removal of mercury from the carrier gas, with a significant flow and the use of a small mass of sorbent. Expanding the research, the authors tried to remove mercury at different temperatures (50, 100, 200, 250 and 300 °C). It is worth mentioning that for the sample MagH-V8-Ag^0, a series of five regeneration cycles were carried out, after which the efficiency of mercury removal decreased only slightly. This may be of key importance in terms of the economic effectiveness of the production and use of a sorbent. The authors identified a combination of the Mars–Maessen mechanism and amalgamation as main mechanism responsible for mercury capture.

In Wdowin et al. (2015), research was undertaken on the most effective of the previously tested zeolites—Ag-loaded Na-X derived from fly ash. In this study, synthetic zeolite X was obtained according to the method described in Franus (2012)—the same method as in the case described above. Raw zeolite X was subjected to the silver ion exchange method using silver nitrate solution (0.5 dm^{-3}, 0.5 mol/dm^3). The textural properties of the activated sample were the same as in the example described above. The study presents two separate mercury removal experiments. Before each test, activated zeolites were dried at 160 °C (10 wt%–12 wt% of moisture was removed from the zeolite in this process). The first test was conducted to confirm the efficiency of the Ag-X zeolite towards Hg^0 removal from the hot air stream. In this experiment, the zeolite sample was placed in two traps. The carrier gas was the hot air stream and the flow rate was set to 0.4 L/min. The temperature of the process was 150 °C and initial mercury concentration was 130 $\mu g/m^3$. After 40 min of the

experiment, the Ag-X mercury removal efficiency was equal to 98%. The second, long-term experiment on Hg uptake by zeolites was carried out using three systems:

(1) 2 × 2 g of powdered zeolite (at 150 °C)
(2) 3 g of granulated zeolite (at 110 °C).

The obtained results indicated an advantage in using the granular form over the powder form of zeolites. The conditions of the mercury removal process carried out on the granulated zeolite Ag-X are shown in Supplementary materials 5 and 6, where 3 g of granulated zeolite was used. The carrier gas was an artificially composed exhaust gas. The flow rate was set to 1.4 L/min. and the process was carried out at 110 °C. The initial mercury concentration was set to approximately 119 μg/m^3. The long-term experiment time was set to 120 min. A 10% breakthrough was observed after 65 min. As mentioned in above study, the main mechanism responsible for Hg^0 is amalgam formation.

In Wdowin et al. (2014b), the use of synthetic zeolites for mercury capture from exhaust gases was described. In this study, the zeolites Na-X and Na-P1 were obtained via a simple hydrothermal reaction of hard coal-derived fly ash with sodium hydroxide. It is worth noting that the preparation of the zeolites was conducted at a one-quarter technical scale using a prototype semi-automatic installation (Wdowin et al. 2014a), and the repeatability was confirmed in numerous experiments. The authors also used a natural zeolite—clinoptilolite from the Sokyrnytsya deposit, Ukraine. Before the Hg^0 removal experiments, all zeolites were dried at 350 °C for 6 h to remove moisture. In order to increase the zeolites' affinity for elemental mercury, whole samples were loaded with silver using the ion exchange method. Na-P1 was also functionalized by melting with $AgNO_3$. XRD quantitative analysis showed that the pure zeolite content in the samples was relatively high, varying from Na-X at 63% to Na-P1 at 81% and clinoptilolite at 95%. The S_{BET} for raw and functionalized zeolites ranged from 260 and 203 m^2/g for Na-X zeolites (raw and Ag-activated) to 88, 53 and 65 m^2/g for Na-P1 zeolites (raw, Ag ion exchange-activated and Ag-melted) and 19 and 14 m^2/g for clinoptilolites (raw and Ag-activated). Total pore volume also varied significantly from 0.22 and 0.16 cm^3/g for Na-X zeolites (raw and Ag-activated) to 0.34, 0.21 and 0.26 cm^3/g for Na-P1 zeolites (raw, Ag ion exchange-activated and Ag-melted) and 0.06 and 0.04 for clinoptilolites (raw and Ag-activated). Average pore diameters were 12.96 and 15.58 nm for Na-X zeolites (raw and Ag-activated), 35.43, 29.73 and 35.18 nm for Na-P1 zeolites (raw, Ag ion exchange-activated and Ag-melted) and 50.60 and 54.75 for clinoptilolites (raw and Ag-activated). For all Ag-loaded zeolites, a reduction in S_{BET} and total pore volume was observed, with a simultaneous increase in the average pore diameter values, indicating that Ag is blocking or filling some of the pores. In the mercury removal experiments, 0.1 g of each sorbent was tested. The carrier gas was pure nitrogen and the gas flow was set to 0.08 L/min, with exception of the sample Na-X/Ag, where the gas flow was 0.16 L/min (due to the high adsorption capacity of the sample). Mercury vapour was generated at 30 °C (± 0.5 °C) and initial mercury concentration was 36 μg/m^3. Raw zeolitic materials were unable to remove more than 10 wt% of mercury. For the untreated zeolites, tests were terminated after 1 h, due to the low uptake efficiency. Results from the Hg^0 removal experiments showed that addition of Ag to the tested samples dramatically improved the performance of the zeolites with respect to mercury capture. The greatest mercury uptake was observed for silver-functionalized zeolite Na-X, since this has the highest BET surface area and the highest combined micropore and mesopore volumes. Approximately four times lower Hg uptake was observed for Ag-loaded Na-P1 zeolite. According to the literature (Moutsatsou et al. 2006) clinoptilolite (both raw and Ag-activated) achieves negligible mercury uptake. Based on the obtained results and on previous work by other authors (Long et al. 1973; Yan 1994; Nowakowski et al. 1997), the authors identified amalgam formation as the main mechanism responsible for mercury capture in silver-loaded zeolites.

4.4 MOFs

Metal-organic frameworks (MOFs) are porous, structurally diverse materials built from the coordinative bonding between metal ions and organic linkers or bridging ligands. MOFs are constructed by anchoring metal-containing units or secondary building units (SBUs) with organic linkers. Binding occurs through coordination, yielding open frameworks that show the exceptional features of durable porosity, stable framework and enormous surface area and pore volume. The presence of long organic linkers leads to relatively high porosity. For this reason, MOFs are characterized by large storage space and many adsorption sites. MOFs also have great potential for functionalizing their structures, allowing their wider application (James 2003; Furukawa et al. 2013; Lu et al. 2014). Supplementary material 7 presents the characteristics of MOFs used recently for elemental mercury removal experiments. Supplementary material 8 shows the experimental parameters and the mechanisms responsible for mercury capture proposed by the cited papers' authors (ordinal numbers from the first column refer to the same samples in both Supplementary material 7 and 8).

In Chen et al. (2018a), a metal-organic framework was synthesized based on 1,3,5-benzenetricarboxylic acid

(H_3BTC). During the synthesis it was functionalized with $Cu(NO_3)_2{\cdot}3H_2O$, to create an affinity for Hg^0. The obtained sorbent was characterized by a high S_{BET} of 1189.69 m^2/g and a total pore volume of 0.53 cm^3/g. The mercury removal experiments used 0.02 g of sorbent. The carrier gas was a mixture of O_2, HCl, SO_2, NO and H_2O. The gas flow rate was set to 0.35 L/min. The test was carried out at a temperature of 150 °C. The initial Hg^0 concentration was 200 $\mu g/m^3$ and the experiment time was set to 120 min. The mercury removal efficiency achieved varied between 93% and 96%. The authors extended their research to include tests on the impact of temperature (25, 50, 75, 100, 200 and 250 °C) and content of HCl and O_2 on the mercury removal process. The following variants were also examined: (a) SO_2, (b) NO, (c) H_2O, (d) coexistence of HCl, SO_2, NO and H_2O with 15 ppm HCl and 10% O_2, (e) SO_2, (f) NO, (g) H_2O and (h) coexistence of HCl, SO_2, NO and H_2O with 5 ppm HCl and 2% O_2. With regard to mercury removal mechanisms, the authors reported that some Hg^0 may be oxidized by active oxygen to HgO when no HCl is present or to $HgCl_2$ by active Cl when HCl is present.

The UiO-67 MOF and ZrO_2 were used as a manganese-cerium catalyst support for Hg^0 and NO removal in Zhang et al. (2017). Materials were obtained by incipient wetness impregnation of MOF with manganese-cerium nitrate. All reagents used in the synthesis came from J&K Scientific Co., Ltd. (Beijing, China). The synthesis procedure is described in more detail in the previous publication by Zhu et al. (2015). The Mn–Ce loaded catalyst was synthesized via incipient wetness impregnation of UiO-67, using $Ce(NO_3)_2$ and $Mn(NO_3)_2$ as precursors, diluted in ethanol. Mn–Ce-impregnated ZrO_2 was obtained by impregnation of 1.5 g of ZrO_2 with cerium and manganese ethanolic solution. The mass ratio was Mn:Ce = 1 and the Mn and Ce loadings were both 5 wt% in the preparation procedure. Undoped MOF has an S_{BET} value of 1376.95 m^2/g, a total pore volume of 0.64 cm^3/g and an average pore diameter of 3.19 nm. The Mn-Ce compound deposited in the pores of the MOF material causes partial blocking of the porous structures in the framework, reducing the surface area and total pore volume. For the activated sample, named MnCe@MOF, the S_{BET} value decreased to 1015.13 m^2/g, the total pore volume was 0.51 cm^3/g and the average pore diameter was 2.01 nm. The textural properties of MnCe@ZrO_2 were much less favourable than those of their predecessors. The S_{BET} value was just 22.88 m^2/g, the total pore volume was 0.05 cm^3/g and the average pore diameter was 8.97 nm. For the mercury removal experiment, 1 g of a given sorbent was used. The carrier gas consisted of O_2, NO and NH_3 in N_2. The flow rate of the carrier gas was set to 0.35 L/min. The process temperature was 300 °C. The initial mercury concentration was 35 $\mu g/m^3$. The experiment time was set to 120 min. Raw MOF was characterized by the lowest efficiency for mercury removal from the carrier gas (about 20%). The MnCe@MOF sample achieved as much as 95% mercury removal and the sample MnCe@ZrO_2 achieved about 80%. The authors also attempted to indicate the optimal temperature for the mercury removal process using the obtained sorbents, by conducting tests over a broad range of temperatures (100, 200, 250, 300 and 350 °C). The influence of oxygen content in the carrier gas was also investigated (zero and 5%). The authors identified adsorption and catalytic oxidation of Hg^0 to HgO as the main mechanisms responsible for mercury removal. Both lattice oxygen and adsorbed oxygen could participate in the catalytic oxidation reaction. In addition, it is worth mentioning that MnCe@MOF and MnCe@ZrO_2 exhibited significant potential for NO removal, which significantly increases the attractiveness of the solution proposed by the authors and increases the likelihood of interest from the energy industry sector.

Removal of Hg^0 from flue gas using open metal sites of Mil-101(Cr) and UiO-66 MOF materials was presented in Zhao et al. (2018). The synthesis was carried out according to the modified procedure described in Bromberg et al. (2012). Chromic nitrate nonahydrate ($Cr(NO_3)_3{\cdot}9H_2O$, $> 99\%$), 1,4-benzenedicarboxylic acid (H_2BDC, 99%) and N,N-dimethylformamide (DMF, 99.5%) were purchased from Aladdin Co., Ltd. (Shanghai, China). Glacial acetic acid (CH_3COOH, $> 99.5\%$) was purchased from Shanghai Ling Feng Chemical Reagent Co., Ltd. (Shanghai, China). The Mil-101(Cr) sample possessed one of the best sets of textural properties described in this article. The S_{BET} was 2487.94 m^2/g and the total pore volume was 0.75 cm^3/g. UiO-66 had a specific surface area of 1090.67 m^2/g and a total pore volume of 0.94 cm^3/g. For the mercury removal experiments, 0.02 g of the sorbents were used. The carrier gas was a mixture of N_2 and O_2. The flow rate was set to 0.5 L/min. and the temperature of the process was 250 °C. The initial concentration of mercury was about 350 $\mu g/m^3$ and the experiment time was set to 500 min. MIL-101(Cr) achieved a very high level of mercury removal efficiency of around 85%, whereas for the sample UiO-66, the efficiency was about 50%. The authors also examined the effect of variable process temperature and oxygen dose (0, 4% and 8%). The process of desorption of entrapped mercury was also analysed. The Hg^0 removal efficiency of MIL-101(Cr) increased with increasing temperature and oxygen content. Based on the XPS and Hg-TPD results, the authors stated that the main mechanisms responsible for mercury removal were adsorption and oxidation via the presence of open metal Cr^{3+} sites. The surface adsorbed oxygen of the adsorbent combined with the generated Hg^{2+} to generate HgO and oxidized the open metal Cr^{2+} site to Cr^{3+}. Excellent results for elemental mercury removal as

well as good chemical and thermal stability are considerable advantages of the proposed solution.

4.5 Others

Among solid sorbents, many other materials have also been tested, some of which are discussed below. Supplementary material 9 presents the characteristics of other sorbents used recently for elemental mercury removal experiments. Supplementary material 10 shows the experimental parameters and the mechanisms responsible for mercury capture proposed by the cited papers' authors (ordinal numbers from the first column refer to the same samples in both Supplementary material 9 and 10).

In Yang et al. (2018a) solid waste resulting from the Bayer process for aluminium production was used. Red mud came from Liaocheng, Shaondong Province, China. The authors reported that at least 160 million Mg of this waste is produced each year in the world. The total stored amount of red mud can be up to 2500 million Mg. These types of landfills are a huge burden on the environment. In this case, the red mud was first dried and then milled and sifted to a particle size of < 50 μm. The red mud was modified via the impregnation method using the potassium halides KI, KBr or KCl. The concentrations of the KI, KBr and KCl solutions were 0.5 wt%, 1 wt% and 3 wt% respectively. The names of the samples in the Supplementary Material 9 refer to these solutions. Raw red mud (RM) had the following textural properties: S_{BET} was 22.49 m^2/g, total pore volume was 0.089 cm^3/g and average pore diameter was 15.50 nm. The micropore surface area was 2.72 m^2/g. The functionalization of RM with both KI and KBr negatively influenced the textural properties of the materials. For samples RMI0.5, RMI1 and RMI3, the S_{BET} values were 21.52, 19.58 and 19.31 m^2/g respectively. Total pore volume decreased accordingly, to 0.086, 0.083 and 0.077 cm^3/g. The micropore surface area values decreased from 2.14 through 1.89 to 0.61 m^2/g. The average pore diameter increased from 15.06, through 18.70 to 18.74 nm. For samples RMB0.5, RMB1 and RMB3, the S_{BET} values were 21.76, 20.64 and 20.23 m^2/g. Total pore volume decreased accordingly, from 0.085 through 0.081 to 0.074 cm^3/g. The micropore surface area values decreased from 2.09, through 1.19 to 1.07 m^2/g. The average pore diameter increased from 15.97, through 17.77 to 18.17 nm. In the elemental mercury removal experiments, 0.2 g samples of given sorbents were used. The carrier gas was a mixture of SO_2, NO, water vapour, O_2 and N_2. The gas carrier flow rate was set to 0.9 L/min, and the temperature of the removal process was 120 °C. The initial Hg^0 concentration was set to 60 $\mu g/m^3$ and the experiment time was set to 90 min. As predicted, the lowest mercury removal efficiency was obtained for the raw RM sample, which achieved an efficiency of 13.8%. For RM functionalization with KI, with an increase in the amount from 0.5% to 3%, the efficiency of mercury removal also increased, from 83.2% up to 94.3%. For RM functionalization with KBr a similar trend was observed. As its amount increased from 0.5% to 3%, the efficiency of mercury removal also increased from 51.3% up to 67.1%. The authors pointed to adsorption on the modified red mud surface, chemisorption and oxidation as the main mechanisms responsible for mercury removal.

In Xu et al. (2018a), hydrothermal synthesis gave three dimensional carbon spheres, α-MnO_2 and MnO_2/CS. Glucose was used as a carbon source. To obtain the carbon spheres, 5.0 g of glucose was dissolved in 100 mL of pure water and then transferred into a 150 mL Teflon hydrothermal synthesis reactor, kept at 200 °C for 10 h. Finally, the product was washed three times with ultrapure water and kept warm at 105 °C for 12 h. In order to obtain MnO_2/CS, 1.0 g of the previously synthesized carbon sphere material was dissolved in pure water under ultrasonic dispersion for 30 min. Then, 5 mmol $MnSO_4 \cdot H_2O$ was added and stirred for 3 h. Subsequently, 5 mmol $KMnO_4$ was slowly added to the above solution and stirred for 1 h. The above mixture was transferred into a Teflon-lined autoclave and maintained at 160 °C for 12 h. The obtained precipitates were washed with water and dried at 8 °C for 12 h. The α-MnO_2 was obtained using the same method but without carbon spheres. The carbon sphere material was characterized by the weakest textural properties. The S_{BET} value barely reached 8.63 m^2/g, the total pore volume was 0.01 cm^3/g and the average pore diameter was 3.35 nm. The α-MnO_2 sample had slightly better textural properties. The S_{BET} was 31.01 m^2/g, the total pore volume was 0.066 cm^3/g and the average pore diameter was 3.69 nm. The best textural properties were recorded for the MnO_2/CS sample. The S_{BET} value reached 134.1 m^2/g, the total pore volume was 0.331 cm^3/g and the average pore diameter was 3.65 nm. In the mercury removal experiments, 0.03 g of the sorbent was used. The carrier gas was pure nitrogen. The measuring system was adapted to perform analyses at a maximum flow rate of 0.5 L/min. Unfortunately, the authors did not give the exact value of the flow rate and the initial mercury concentration for the samples analysed. The experiment was carried out at a temperature of 150 °C and the time was set to 600 min. According to expectations, the smallest affinity for elemental mercury was found in the raw sample of carbon spheres, with about 12% Hg^0 removal efficiency. Better results were obtained from the α-MnO_2 and MnO_2/CS samples. In these samples, the obtained efficiencies were 91.73% and 95.6% respectively for removal of Hg^0. The authors also conducted studies on the impact of temperature on the mercury removal efficiency (in the range

100–350 °C). As the temperature increased, the efficiency of Hg^0 removal in the α-MnO_2 sample decreased significantly (64.8% at 250 °C, 56.85% at 300 °C and 28% at 350 °C). For the MnO_2/CS sample there was also a decrease in mercury removal efficiency with a rise in temperature: at 300°C the efficiency was 72.16%, dropping to 30.6% at 350 °C. This shows that such high temperatures significantly adversely affect the process of elemental mercury removal in manganese oxide-based materials. Adsorption and oxidation processes were identified as the main mechanisms responsible for mercury capture.

5 Research gap summary and future research directions

Due to physicochemical properties of mercury which give it a number of features such as high toxicity and bioaccumulation, Hg emissions from energy sector remains a hazardous threat to human beings and environment. In last years, both industry and scientists have put significant effort in order to develop new techniques that help reduce mercury emissions into the environment. However, new law regulations and restrictions regarding emission levels mean that there is still space for new works and solutions, due to the fact that actually existing solutions don't meet new requirements. Considering literature concluded and cited in this paper it can be stated that there is a research gap of possibility to compare individual types of sorbents and their effectiveness in relation to Hg removal. The multitude and divergence of parameters and variable systems in which the described tests were conducted makes it impossible to accurately compare sorbents. Studies showing a comparison of a number of sorbents tested under equal conditions would have an invaluable value. Hg^0 constitute about 90% of all mercury in exhaust gases and it is also the most difficult to be removed there is a great need for further research towards searching for a new way of removal. In addition, the analysis presented so far focused mainly on laboratory results under simulated conditions, so there is a lack of tests in real conditions that would give a real view of the effectiveness of these sorbents. As long as the economies of many countries will be based on energy obtained from the combustion of solid fuels research and work will still be needed in order to obtain novel, more effective, cheaper, less environment harmful sorbents capable of removing of mercury.

Generally, based on the reviewed literature, the following research is worth to carrying out in the future:

(1) The effects of flue gas components, especially SO_2 and NO on Hg^0 uptake depending on the type of sorbent;
(2) Interoperability of laboratory methods mercury control with large-scale demonstration projects in coal-fired power plants;
(3) The influence of adsorbent injection temperature and rate on Hg0 removal efficiency important from the point of view of use in ESP (electrostatic precipitator) or FF (fabric filter) systems in power plants;
(4) The mathematical models based on available laboratory tests and simulations of the impact of variables such as flue gas chemistry, mass transfer, physical and chemical adsorption on the efficiency of Hg^0 removal;
(5) Economic analysis of the profitability of implementing the proposed solution for power plants
(6) The comprehensive and systematic economy analysis taking into account the costs of adsorbent regeneration and its management after use.

6 Conclusions

The aim of the research in this paper is to present a compendium of novel solid sorbent solutions dedicated to the removal of elemental mercury from gases. The paper discusses a wide spectrum of recently obtained materials which have achieved very promising results in Hg^0 removal experiments. Among them are materials such as activated carbons, biochars, zeolites and metal-organic frameworks. The origins of the materials or the methods of their production have been given, as well as methods of modification aiming was to increase the affinity for elemental mercury. The dominant method for functionalizing materials was impregnation, while silver, cerium and manganese compounds were the substances most often used for activation. Some of the presented materials were purchased, while others were produced in laboratory or at a one-quarter technical scale. As far as possible, textural characteristics, including the most influential properties (S_{BET}, total pore volume, micropore volume and average pore diameter) have also been presented. In order to obtain the most complete view of the proposed sorbents, as many as possible of the mercury removal experiment parameters are given, including the mass of sorbent, the carrier gas composition, the flow rate, the temperature at which the Hg^0 removal process was carried out, the initial mercury concentration in the gas and the time for 10% breakthrough or the whole duration of the experiment, as well as the sorbent efficiency given as a percentage. Finally, an indication of the mechanisms responsible for mercury capture was given. This paper presents only the most effective proposed sorbents. In some cases, the development of the experiments was also discussed—most of the cited papers included a description of the selection of the appropriate

process temperature, as well as the impact of the individual components of the carrier gas, (e.g., O_2, SO_2, NO and H_2O) on Hg^0 removal efficiency.

The analysis carried out indicates that the best result was achieved by the MOF samples MIL-101(Cr) and UiO-66 (Zhao et al. 2018). Very promising results were also achieved by a number of activated carbons doped with gold nanoparticles (Rodríguez-Pérez et al. 2011). The decisive disadvantage of these solutions is the cost of production and functionalization of sorbents. Zeolites seem to provide an interesting and more economical solution. However, in this case, silver activation also increases the total cost of sorbent production (Wdowin et al. 2014b, 2015; Cao et al. 2017). Some of the described solutions achieved very interesting, economically effective and high-efficiency results that possess high potential for application and certainly deserve further development and greater interest from the energy industry sector.

Acknowledgements This work was supported by the National Centre for Research and Development project LIDER, Contract Number LIDER/384/L-6/14/NCBR/2015.

Authors' contributions PK: Conceptualization, Draft preparation, Writing-Reviewing and Editing, Visualization. DCJ: Conceptualization, Draft preparation, Writing-Reviewing and Editing, Visualization. MW: Supervision, Project Administration, Funding acquisition.

Compliance with ethical standards

Conflict of interest The authors declared that they have no conflict of interest.

References

Aguilar-Mamani W, García G, Hedlund J, Mouzon J (2014) Comparison between leached metakaolin and leached diatomaceous earth as raw materials for the synthesis of ZSM-5. SpringerPlus 292:1–10

Ahmaruzzaman M (2010) A review on the utilization of fly ash. Prog Energy Combust Sci 36:327–363. https://doi.org/10.1016/j.pecs.2009.11.003

Ahmed MJ, Theydan SK (2012) Physical and chemical characteristics of activated carbon prepared by pyrolysis of chemically treated date stones and its ability to adsorb organics. Powder Technol 229:237–245. https://doi.org/10.1016/j.powtec.2012.06.043

AMAP (2008) Technical background report to the global atmospheric mercury assessment. Arctic Monitoring and Assessment Programme/UNEP Chemicals Branch, Olso

Amaya A, Medero N, Tancredi N et al (2007) Activated carbon briquettes from biomass materials. Bioresour Technol 98:1635–1641. https://doi.org/10.1016/j.biortech.2006.05.049

Baçaoui A, Yaacoubi A, Dahbi A et al (2001) Optimization of conditions for the preparation of activated carbons from olive-waste cakes. Carbon N Y 39:425–432. https://doi.org/10.1016/S0008-6223(00)00135-4

Baerlocher C, McCusker LB, Olson DH (2007) Atlas of zeolite framework types. Sixth revised edn. Published on behalf of thestructure Commission of the international Zeolite Association. Elsevier, The Netherlands

Bhardwaj R, Chen X, Vidic RD (2009) Impact of fly ash composition on mercury speciation in simulated flue gas. J Air Waste Manag Assoc 59:1331–1338. https://doi.org/10.3155/1047-3289.59.11.1331

Boycheva S, Zgureva D, Shoumkova A (2014) Recycling of lignite coal fly ash by its conversion into zeolites. Coal Combust Gasif Prod 6:1–8. https://doi.org/10.4177/CCGP-D-14-00008.1

Bromberg L, Diao Y, Wu H et al (2012) Chromium(III) terephthalate metal organic framework (MIL-101): HF-free synthesis, structure, polyoxometalate composites, and catalytic properties. Chem Mater 24:1664–1675. https://doi.org/10.1021/cm2034382

Brown TD, Smith DN, Hargis RA Jr et al (1999) Mercury measurement and its control: what we know, have learned, and need to further investigate. J Air Waste Manag Assoc 2247:628–640. https://doi.org/10.1080/10473289.1999.10463841

Bujny M, Burmistrz P, Gruszka S et al (2012) Instalacja demonstracyjna do monitorowania i redukcji emisji rtęci ze spalania węgla kamiennego w kotłach pyłowych. Polityka Energ 15:161

Burmistrz P, Bytnar K, Kogut K et al (2008) Wiarygodność wyników badań węgla kamiennego. Gospod Surowcami Miner 24:33–48

Burmistrz P, Czepirski L, Kogut K, Strugała A (2014) Removing mercury from flue gases. A demo plant based on injecting dusty sorbents. Chem Ind 12:2014–2019

Burriesci N, Crisafulli ML, Saija LM, Polizzotti G (1983) Hydrothermal synthesis of zeolites from rhyolitic pumice of different geological origins. Mater Lett 2:74–78

Cao T, Zhou Z, Chen Q et al (2017) Magnetically responsive catalytic sorbent for removal of Hg^0 and NO. Fuel Process Technol 160:158–169. https://doi.org/10.1016/j.fuproc.2017.02.022

Chen J, Yuan D, Li Q et al (2008) Effect of flue-gas cleaning devices on mercury emission from coal-fired boiler. Proc Chin Soc Electr Eng 28:72–76

Chen D, Zhao S, Qu Z, Yan N (2018a) Cu-BTC as a novel material for elemental mercury removal from sintering gas. Fuel 217:297–305. https://doi.org/10.1016/j.fuel.2017.12.086

Chen J, Li C, Li S et al (2018b) Simultaneous removal of HCHO and elemental mercury from flue gas over Co–Ce oxides supported on activated coke impregnated by sulfuric acid. Chem Eng J 338:358–368. https://doi.org/10.1016/j.cej.2018.01.043

Chmielewski AG (2004) Environmental effects of fossil fuel combustion. In: Goldember J (ed) Interactions: Energy/Environment. United Nations Educational, Scientific and Cultural Organization, pp 56–74

Chmielniak T, Głód K, Misztal E, Kopiczyński M (2010) mercury emission from caol-fired power plants. Przem Chem 89:775–778

Council E (2010) Directive 2010/75/EU industrial emissions. Off J Eur Union L334:17–119. https://doi.org/10.3000/17252555.L_2010.334.eng

Czarna D, Baran P, Kunecki P et al (2016) Synthetic zeolites as potential sorbents of mercury from wastewater occurring during wet FGD processes of flue gas. J Clean Prod 172:2636–2645. https://doi.org/10.1016/j.jclepro.2017.11.147

Dastoor AP, Larocque Y (2004) Global circulation of atmospheric mercury: a modelling study. Atmos Environ 38:147–161. https://doi.org/10.1016/j.atmosenv.2003.08.037

Demiral H, Demiral I, Tümsek F, Karabacakoğlu B (2008) Pore structure of activated carbon prepared from hazelnut bagasse by chemical activation. Surf Interface Anal 40:616–619. https://doi.org/10.1002/sia.2631

Dunham GE, DeWall RA, Senior CL (2003) Fixed-bed studies of the interactions between mercury and coal combustion fly ash. Fuel Process Technol 82:197–213. https://doi.org/10.1016/S0378-3820(03)00070-5

EEA (2016) Air quality in Europe: 2016 report. European Environment Agency EEA

Eldien IM, Al-Sarawy AA, El-Halwany MM, El-Msaly FR (2016) Kinetics and thermodynamics evaluation of activated carbon derived from peanuts shell as a sorbent material. J Chem Eng Process Technol 07:1–7. https://doi.org/10.4172/2157-7048.1000267

European Commission (1998) Council directive 98/83/EC, Ammended by EC 2015/1787 of 6 Oct 2015

Fan X, Li C, Zeng G et al (2010) Removal of gas-phase element mercury by activated carbon fiber impregnated with CeO_2. Energy Fuels 24:4250–4254. https://doi.org/10.1021/ef100377f

Fiałkowski M, Grzeszczak P, Nowakowski R, Hołyst R (2004) Absorption of mercury in gold films and its further desorption: quantitative morphological study of the surface patterns. J Phys Chem B 108:5026–5030. https://doi.org/10.1021/jp0365413

Franus W (2012) Characterization of X-type zeolite prepared from coal fly ash. Pol J Environ Stud 21:337–343. https://doi.org/10.1016/j.chemosphere.2012.06.012

Franus W, Wdowin M, Franus M (2014) Synthesis and characterization of zeolites prepared from industrial fly ash. Environ Monit Assess 186:5721–5729. https://doi.org/10.1007/s10661-014-3815-5

Franus M, Wdowin M, Bandura L, Franus W (2015) Removal of environmental pollutions using zeolites from fly ash: a review. Fresenius Environ Bull 24:854–866

Fu X, Feng X, Sommar J, Wang S (2012) A review of studies on atmospheric mercury in China. Sci Total Environ 421–422:73–81. https://doi.org/10.1016/j.scitotenv.2011.09.089

Furukawa H, Cordova KE, O'Keeffe M, Yaghi OM (2013) The chemistry and applications of metal-organic frameworks. Science (80-) 341:1230444

Galbreath KC, Zygarlicke CJ (2000) Mercury transformations in coal combustion flue gas. Fuel Process Technol 65:289–310. https://doi.org/10.1016/S0378-3820(99)00102-2

Gale TK, Lani BW, Offen GR (2008) Mechanisms governing the fate of mercury in coal-fired power systems. Fuel Process Technol 89:139–151. https://doi.org/10.1016/j.fuproc.2007.08.004

Gao Y, Zhang Z, Wu J et al (2013) A critical review on the heterogeneous catalytic oxidation of elemental mercury in flue gases. Environ Sci Technol 47:10813–10823. https://doi.org/10.1021/es402495h

Garcia G, Cardenas E, Cabrera S, Hedlund J (2016) Microporous and mesoporous materials synthesis of zeolite Y from diatomite as silica source. Microporous Mesoporous Mater 219:29–37. https://doi.org/10.1016/j.micromeso.2015.07.015

Gerasimov G (2005) Investigation of the behavior of mercury compounds in coal combustion products. J Eng Thermophys 78:668–676

Guo Y, Rockstraw DA (2007) Physicochemical properties of carbons prepared from pecan shell by phosphoric acid activation. Bioresour Technol 98:1513–1521. https://doi.org/10.1016/j.biortech.2006.06.027

Gustin MS, Lindberg SE, Weisberg PJ (2008) An update on the natural sources and sinks of atmospheric mercury. Appl Geochem 23:482–493. https://doi.org/10.1016/j.apgeochem.2007.12.010

Hall B, Schager P, Lindqvist O (1991) Chemical-reactions of mercury in combustion flue-gases. Water Air Soil Pollut 56:3–14. https://doi.org/10.1007/bf00342256

Handke M (2008) Krystalochemia krzemianów. Uczelniane Wydawnictwo Naukowo-Dydaktyczne AGH im. S. Staszica, Kraków

Hassett DJ, Heebink LV, Pflughoeft-Hassett DF (1999) Potential for mercury vapor release from coal combustion by-products. Fuel Proc Technol 85:613–620

Hassett DJ, Heebink LV, Pflughoeft-Hassett DF (2004) Potential for mercury vapor release from coal combustion by-products. Fuel Process Technol 85:613–620. https://doi.org/10.1016/j.fuproc.2003.11.010

Heebink LV, Hassett DJ (2002) Release of mercury vapor from coal combustion ash. J Air Waste Manag Assoc 52:927–930. https://doi.org/10.1080/10473289.2002.10470828

Holmes SM, Khoo SA, Kovo AS (2011) The direct conversion of impure natural kaolin into pure zeolite catalysts. Green Chem 13:1152–1154

Hou T, Chen M, Greene GW, Horn RG (2015) Mercury vapor sorption and amalgamation with a thin gold film. ACS Appl Mater Interfaces 7:23172–23181. https://doi.org/10.1021/acsami.5b07002

International Energy Agency (2017) Market report series. Coal 2017

James SL (2003) Metal: organic frameworks. Chem Soc Rev 32:276–288

Johnson EBG, Arshad SE (2014) Hydrothermally synthesized zeolites based on kaolinite: a review. Appl Clay Sci 97–98:215–221. https://doi.org/10.1016/j.clay.2014.06.005

Kadirvelu K, Kavipriya M, Karthika C et al (2004) Mercury(II) adsorption by activated carbon made from sago waste. Carbon N Y 42:745–752. https://doi.org/10.1016/j.carbon.2003.12.089

Kemp KC, Bin BS, Lee WG et al (2015) Activated carbon derived from waste coffee grounds for stable methane storage. Nanotechnology. https://doi.org/10.1088/0957-4484/26/38/385602

Khadiran T, Hussein MZ, Zainal Z, Rusli R (2015) Activated carbon derived from peat soil as a framework for the preparation of shape-stabilized phase change material. Energy 82:468–478. https://doi.org/10.1016/j.energy.2015.01.057

Kumari R (2011) Emission estimate of passport-free heavy metal mercury from Indian thermal power plants and non-ferrous smelters. Toxic Links. European Environmental Bureau – Zero Mercury Campaign

Kunecki P, Panek R, Wdowin M, Franus W (2017) Synthesis of faujasite (FAU) and tschernichite (LTA) type zeolites as a potential direction of the development of lime Class C fly ash. Int J Miner Process 166:69–78. https://doi.org/10.1016/j.minpro.2017.07.007

Kunecki P, Panek R, Koteja A, Franus W (2018) Influence of the reaction time on the crystal structure of Na-P1 zeolite obtained from coal fly ash microspheres. Microporous Mesoporous Mater 266:102–108. https://doi.org/10.1016/j.micromeso.2018.02.043

Lavoie RA, Jardine TD, Chumchal MM et al (2013) Biomagnification of mercury in aquatic food webs: a worldwide meta-analysis. Environ Sci Technol 47:13385–13394. https://doi.org/10.1021/es403103t

Le Van K, Luong Thi TT (2014) Activated carbon derived from rice husk by NaOH activation and its application in supercapacitor. Prog Nat Sci Mater Int 24:191–198. https://doi.org/10.1016/j.pnsc.2014.05.012

Lecomte T, Ferrería De La Fuente FJ, Neuwahl F, et al (2017) Best available techniques (BAT) reference document for large combustion plants: industrial emissions directive 2010/75/EU (integrated pollution prevention and control)

Lindberg S, Bullock R, Ebinghaus R et al (2007) A synthesis of progress and uncertainties in attributing the sources of mercury in deposition. Ambio 36:19–32. https://doi.org/10.1579/0044-7447(2007)36%5b19:ASOPAU%5d2.0.CO;2

Liu Z, Yang W, Xu W, Liu Y (2018) Removal of elemental mercury by bio-chars derived from seaweed impregnated with potassium iodine. Chem Eng J 339:468–478. https://doi.org/10.1016/j.cej.2018.01.148

Long SJ, Scott DR, Thompson RJ (1973) Atomic absorption determination of elemental mercury collected from ambient air on silver wool. Anal Chem 45:2227–2233. https://doi.org/10.1021/ac60335a032

López FA, Centeno TA, Rodríguez O, Alguacil FJ (2013) Preparation and characterization of activated carbon from the char produced in the thermolysis of granulated scrap tyres. J Air Waste Manag Assoc 63:534–544. https://doi.org/10.1080/10962247.2013.763870

Lopez-Anton MA, Yuan Y, Perry R, Maroto-Valer MM (2010) Analysis of mercury species present during coal combustion by thermal desorption. Fuel 89:629–634. https://doi.org/10.1016/j.fuel.2009.08.034

Lu W, Wei Z, Gu Z-Y et al (2014) Tuning the structure and function of metal–organic frameworks via linker design. Chem Soc Rev 43:5561–5593

Mahaffey KR, Sunderland EM, Chan HM et al (2012) Balancing the benefits of n-3 polyunsaturated fatty acids and the risks of methylmercury exposure from fish consumption. Nutr Rev 69:493–508. https://doi.org/10.1111/j.1753-4887.2011.00415.x. Balancing

Manyà JJ (2012) Pyrolysis for biochar purposes: a review to establish current knowledge gaps and research needs. Environ Sci Technol 46:7939–7954

Mills SJ (2007) Prospects for coal and clean coal technologies in India. CCC/161. London, UK, IEA Clean Coal Centre

Mohamed MM (2008) Synthesis of ZSM-5 zeolite from rice husk ash: characterization and implications for photocatalytic degradation catalysts. Microporous Mesoporous Mater 108:193–203. https://doi.org/10.1016/j.micromeso.2007.03.043

Mohamed RM (2015) Rice husk ash as a renewable source for the production of zeolite NaY and its characterization. Arab J Chem 8:48–53. https://doi.org/10.1016/j.arabjc.2012.12.013

Morency JR, Panagiotou T, Senior CL (2000) Laboratory duct injection of a zeolite-based mercury sorbent. In: Presented at the Annual Meeting of the Air & Waste Management Association, Salt Lake City, UT, June 2000. Physical Sciences Inc., Andover, MA

Moutsatsou A, Stamatakis E, Hatzitzotzia K, Protonotarios V (2006) The utilization of Ca-rich and Ca–Si-rich fly ashes in zeolites production. Fuel 85:657–663. https://doi.org/10.1016/j.fuel.2005.09.008

Namasivayam C, Sangeetha D (2006) Recycling of agricultural solid waste, coir pith: removal of anions, heavy metals, organics and dyes from water by adsorption onto $ZnCl_2$ activated coir pith carbon. J Hazard Mater 135:449–452. https://doi.org/10.1016/j.jhazmat.2005.11.066

Niksa S, Helble JJ, Fujiwara N (2001) Kinetic modeling of homogeneous mercury oxidation: the importance of NO and H_2O in predicting oxidation in coal-derived systems. Environ Sci Technol 35:3701–3706

Norton GA, Yang H, Brown RC et al (2003) Heterogeneous oxidation of mercury in simulated post combustion conditions. Fuel 82:107–116. https://doi.org/10.1016/S0016-2361(02)00254-5

Nowakowski R, Kobiela T, Wolfram Z, Duś R (1997) Atomic force microscopy of Au/Hg alloy formation on thin Au films. Appl Surf Sci 115:217–231. https://doi.org/10.1016/S0169-4332(96)01091-4

Olkuski T (2007) Porównanie zawartoœci rtęci w węglach polskich i amerykańskich. Polityka Energetyczna 10:603–611

Ospanov K, Myrzakhmetov M, Andraka D, Dzienis L (2016) Application of natural zeolite for intensification of municipal wastewater treatment. J Ecol Eng 17:57–63. https://doi.org/10.12911/22998993/65446

Panagiotou T, Morency JR, Senior CL (2000) Zeolite-based mercury sorbent-laboratory testing and modeling. ACS Div Fuel Chem Prepr 45:426–430

Panek R, Wdowin M, Franus W et al (2017) Fly ash-derived MCM-41 as a low-cost silica support for polyethyleneimine in post-combustion CO_2 capture. J CO2 Util 22:81–90. https://doi.org/10.1016/j.jcou.2017.09.015

Park KS, Seo YC, Lee SJ, Lee JH (2008) Emission and speciation of mercury from various combustion sources. Powder Technol 180:151–156. https://doi.org/10.1016/j.powtec.2007.03.006

Pavlish JH, Sondreal EA, Mann MD et al (2003) Status review of mercury control options for coal-fired power plants. Fuel Process Technol 82:89–165. https://doi.org/10.1016/S0378-3820(03)00059-6

Pavlish JH, Hamre LL, Zhuang Y (2010) Mercury control technologies for coal combustion and gasification systems. Fuel 89:838–847. https://doi.org/10.1016/j.fuel.2009.05.021

Pichór W, Król M, Mozgawa W (2015) Lightweight zeolites from the aluminosilicate fillers. In: International conference of the european ceramic society, 21–25 June, 2015, Toledo, España

Pirrone N, Cinnirella S, Feng X et al (2009) Global mercury emissions to the atmosphere from natural and anthropogenic sources. Mercur Fate Transp Glob Atmos Emiss Meas Model. https://doi.org/10.1007/978-0-387-93958-2_1

Prestbo EM, Bloom NS (1995) Mercury speciation adsorption (MESA) method for combustion flue gas: methodology, artifacts, intercomparison, and atmospheric implications. Water Air Soil Pollut 80:145–158. https://doi.org/10.1007/BF01189663

Presto AA, Granite EJ (2006) Survey of catalysts for oxidation of mercury in flue gas. Environ Sci Technol 40:5601–5609. https://doi.org/10.1021/es060504i

Qi H, Xu W, Wang J et al (2015) Hg0 removal from flue gas over different zeolites modified by $FeCl_3$. J Environ Sci 28:110–117

Ríos CA, Williams CD, Castellanos OM (2012) Crystallization of low silica Na-A and Na-X zeolites from transformation of kaolin and obsidian by alkaline fusion cristalizacion de zeolitas Na-A y Na-X bajas en sílice a partir de la transformación de caolín y obsidiana por fusión alcalina. Ing Compet 14:125–137

Rodríguez-Pérez J, López-Antón MA, Díaz-Somoano M et al (2011) Development of gold nanoparticle-doped activated carbon sorbent for elemental mercury. Energy Fuels 25:2022–2027. https://doi.org/10.1021/ef2001053

Ryzhov VV, Mashyanov NR, Ozerova NA, Pogarev SE (2003) Regular variations of the mercury concentration in natural gas. Sci Total Environ 304:145–152. https://doi.org/10.1016/S0048-9697(02)00564-8

Schroeder WH, Munthe J (1998) Atmospheric mercury: an overview. Atmos Environ 32:809–822. https://doi.org/10.1016/S1352-2310(97)00293-8

Senior CL, Sarofim AF, Zeng T et al (2000) Gas-phase transformations of mercury in coal-fired power plants. Fuel Process Technol 63:197–213. https://doi.org/10.1016/S0378-3820(99)00097-1

Shewchuk SR, Azargohar R, Dalai AK (2016) Elemental mercury capture using activated carbon: a review. J Environ Anal Toxicol. https://doi.org/10.4172/2161-0525.1000379

Silva HS, Ruiz SV, Granados DL, Santángelo JM (2010) Adsorption of mercury(II) from liquid solutions using modified activated carbons. Mater Res 13:129–134. https://doi.org/10.1590/S1516-14392010000200003

Sjostrom S, Durham M, Bustard CJ, Martin C (2010) Activated carbon injection for mercury control: overview. Fuel 89:1320–1322. https://doi.org/10.1016/j.fuel.2009.11.016

Sloss LL (2012) Mercury emissions from India and South East Asia. United Nations Environment Programme. US Department of State. ARCADIS. S-LMAQM-11-GR-1009

Srogi K (2007) Technologie obniżania emisji rtęci z węgla. Wiadomości Górnicze 58:575–580

Sterling R, Qiu J, Helble JJ (2004) Experimental study of mercury post-flame conditions. In: The 227th spring ACS national meeting, pp 277–278

Sun H, Zhao S, Ma Y et al (2018) Effective and regenerable Ag/4A zeolite nanocomposite for Hg^0 removal from natural gas. J Alloys Compd 762:520–527. https://doi.org/10.1016/j.jallcom.2018.05.222

Tan Z, Sun L, Xiang J et al (2012) Gas-phase elemental mercury removal by novel carbon-based sorbents. Carbon N Y 50:362–371. https://doi.org/10.1016/j.carbon.2011.08.036

Tsujiguchi M, Kobashi T, Oki M et al (2014) Synthesis and characterization of zeolite A from crushed particles of aluminoborosilicate glass used in LCD panels. J Asian Ceram Soc 2:27–32. https://doi.org/10.1016/j.jascer.2013.12.005

UNEP (2011) Annual report 2011

UNEP (2013a) Global mercury assessment 2013. Sources, emissions, releases and environmental transport

UNEP (2013b) Minamata convention on mercury: text and annexes

US EPA (2002) Control of mercury emissions from coal-fired electric utility boilers: interim report including errata dated 3-21-02

Veiga MM, Maxson PA, Hylander LD (2006) Origin and consumption of mercury in small-scale gold mining. J Clean Prod 14:436–447. https://doi.org/10.1016/j.jclepro.2004.08.010

Wang SX, Zhang L, Li GH et al (2010) Mercury emission and speciation of coal-fired power plants in China. Atmos Chem Phys 10:1183–1192. https://doi.org/10.5194/acp-10-1183-2010

Wang Y, Li C, Zhao L et al (2016) Study on the removal of elemental mercury from simulated flue gas by Fe_2O_3–CeO_2/AC at low temperature. Environ Sci Pollut Res 23:5099–5110. https://doi.org/10.1007/s11356-015-5717-7

Wang T, Liu J, Zhang Y et al (2018) Use of a non-thermal plasma technique to increase the number of chlorine active sites on biochar for improved mercury removal. Chem Eng J 331:536–544. https://doi.org/10.1016/j.cej.2017.09.017

Wdowin M, Franus M, Panek R et al (2014a) The conversion technology of fly ash into zeolites. Clean Technol Environ Policy 16:1217–1223. https://doi.org/10.1007/s10098-014-0719-6

Wdowin M, Wiatros-Motyka MM, Panek R et al (2014b) Experimental study of mercury removal from exhaust gases. Fuel 128:451–457. https://doi.org/10.1016/j.fuel.2014.03.041

Wdowin M, Macherzyński M, Panek R et al (2015) Investigation of the sorption of mercury vapour from exhaust gas by an Ag-X zeolite. Clay Miner 50:31–40. https://doi.org/10.1180/claymin.2015.050.1.04

WEC (2016) World energy resources 2016

Widmer NC, West J, Cole JA (2000) Thermochemical study of mercury oxidation in utility boiler fuel gases. In: 93rd Annual Meeting, Air & Waste Management Association, Salt Lake City, UT

Wojnar K, Wisz J (2006) Rtęć w polskiej energetyce. Energetyka 4:280–283

Wu Y, Wang S, Streets DG et al (2006) Trends in anthropogenic mercury emissions in china from 1995 to 2003. Environ Sci Technol 40:5312–5318

Wu J, Zhao Z, Huang T et al (2017) Removal of elemental mercury by Ce–Mn co-modified activated carbon catalyst. Catal Commun 93:62–66. https://doi.org/10.1016/j.catcom.2017.01.016

Xie Y, Li C, Zhao L et al (2015) Experimental study on Hg^0 removal from flue gas over columnar MnO_x–CeO_2 activated coke. Appl Surf Sci 333:59–67. https://doi.org/10.1016/j.apsusc.2015.01.234

Xu P, Zeng GM, Huang DL et al (2012) Use of iron oxide nanomaterials in wastewater treatment: a review. Sci Total Environ 424:1–10. https://doi.org/10.1016/j.scitotenv.2012.02.023

Xu W, Wang H, Zhou X, Zhu T (2014) CuO/TiO_2 catalysts for gas-phase Hg^0 catalytic oxidation. Chem Eng J 243:380–385. https://doi.org/10.1016/j.cej.2013.12.014

Xu H, Jia J, Guo Y et al (2018a) Design of 3D MnO_2/Carbon sphere composite for the catalytic oxidation and adsorption of elemental mercury. J Hazard Mater 342:69–76. https://doi.org/10.1016/j.jhazmat.2017.08.011

Xu W, Adewuyi YG, Liu Y, Wang Y (2018b) Removal of elemental mercury from flue gas using CuO_x and CeO_2 modified rice straw chars enhanced by ultrasound. Fuel Process Technol 170:21–31. https://doi.org/10.1016/j.fuproc.2017.10.017

Yamaguchi A, Akiho H, Ito S (2008) Mercury oxidation by copper oxides in combustion flue gases. Powder Technol 180:222–226. https://doi.org/10.1016/j.powtec.2007.03.030

Yan T (1994) A novel process for Hg removal from gases. Ind Eng Chem Res 33:3010–3014. https://doi.org/10.1021/ie00036a016

Yang H, Xu Z, Fan M et al (2007) Adsorbents for capturing mercury in coal-fired boiler flue gas. J Hazard Mater 146:1–11. https://doi.org/10.1016/j.jhazmat.2007.04.113

Yang W, Hussain A, Zhang J, Liu Y (2018a) Removal of elemental mercury from flue gas using red mud impregnated by KBr and KI reagent. Chem Eng J 341:483–494. https://doi.org/10.1016/j.cej.2018.02.023

Yang W, Liu Z, Xu W, Liu Y (2018b) Removal of elemental mercury from flue gas using sargassum chars modified by NH4Br reagent. Fuel 214:196–206. https://doi.org/10.1016/j.fuel.2017.11.004

Yi W, Zhu X, Qi W (2017) Technology of biomass pyrolysis. In: Yuan Z (ed) Bioenergy: principles and technologies, vol 2.2. De Gruyter

Yi Y, Li C, Zhao L et al (2018) The synthetic evaluation of CuO–MnO_x-modified pinecone biochar for simultaneous removal formaldehyde and elemental mercury from simulated flue gas. Environ Sci Pollut Res 25:4761–4775. https://doi.org/10.1007/s11356-017-0855-8

Yudovich YE, Ketris MP (2005) Mercury in coal: a review. Part 1. Geochemistry. Int J Coal Geol 62:107–134. https://doi.org/10.1016/j.coal.2004.11.002

Zhang L, Zhuo Y, Chen L et al (2008) Mercury emissions from six coal-fired power plants in China. Fuel Process Technol 89:1033–1040. https://doi.org/10.1016/j.fuproc.2008.04.002

Zhang L, Daukoru M, Torkamani S et al (2013) Measurements of mercury speciation and fine particle size distribution on combustion of China coal seams. Fuel 104:732–738. https://doi.org/10.1016/j.fuel.2012.06.069

Zhang L, Wang S, Wu Q et al (2016) Mercury transformation and speciation in flue gases from anthropogenic emission sources: a critical review. Atmos Chem Phys 16:2417–2433. https://doi.org/10.5194/acp-16-2417-2016

Zhang X, Shen B, Shen F et al (2017) The behavior of the manganese-cerium loaded metal-organic framework in elemental mercury and NO removal from flue gas. Chem Eng J 326:551–560. https://doi.org/10.1016/j.cej.2017.05.128

Zhao L, Huang Y, Chen H et al (2017) Study on the preparation of bimetallic oxide sorbent for mercury removal. Fuel 197:20–27. https://doi.org/10.1016/j.fuel.2017.01.122

Zhao S, Mei J, Xu H et al (2018) Research of mercury removal from sintering flue gas of iron and steel by the open metal site of Mil-101(Cr). J Hazard Mater 351:301–307. https://doi.org/10.1016/j.jhazmat.2017.12.016

Zhu X, Li B, Yang J et al (2015) Effective adsorption and enhanced removal of organophosphorus pesticides from aqueous solution by Zr-based MOFs of UiO-67. ACS Appl Mater Interfaces 7:223–231